water

MDPI

Article

Strategy for Flux Enhancement in Biofilm Ceramic Membrane Bioreactor Applying Prepolymerized and Non-Prepolymerized Inorganic Coagulants

Olga Kulesha [1,2,*], Zakhar Maletskyi [1], Knut Kvaal [1] and Harsha Ratnaweera [1]

[1] Faculty of Science and Technology (REALTEK), Norwegian University of Life Sciences, PO Box 5003, 1432 Aas, Norway; zakhar.maletskyi@nmbu.no (Z.M.); knut.kvaal@nmbu.no (K.K.); harsha.ratnaweera@nmbu.no (H.R.)

[2] Department of General and Inorganic Chemistry, Faculty of Chemical Technology, National Technical University of Ukraine "Igor Sikorsky Kyiv Polytechnic Institute", Peremohy 37, 03056 Kyiv, Ukraine

* Correspondence: olga.kulesha@nmbu.no; Tel.: +47-406-755-92

Received: 11 February 2019; Accepted: 22 February 2019; Published: 2 March 2019

Abstract: Considering new legislative and economic restrictions caused by the water crisis, this work focuses on a more efficient wastewater treatment process, which combines biological treatment in a moving bed biofilm system with a membrane bioreactor (BF-MBR) and coagulation, particularly addressing fouling alleviation in the separation stage. The study justifies the positive impact of coagulant dosing in BF-MBR regarding membrane flux and fouling rate. Statistical techniques connect the results of coagulation and membrane separation experiments with properties of mixed liquor, obtained after biotreatment in the representative pilot plant and characteristics of prepolymerized and non-prepolymerized inorganic coagulants. Research results substantiate the need for a pH-controlled coagulation of mixed liquor in BF-MBR depending on coagulant type, which influences charge, hydrophobicity and size of flocs and organic content of the system. It is suggested, that the adsorption/charge neutralization mechanism dominates in flux enhancement in BF-MBR, giving the best results in the case of prepolymerized aluminium coagulants. Together with high quality of permeate, the application of prepolymerized aluminium chloride of medium basicity entails a tenfold increase in filtration time of the membrane separation cycle and increases net membrane flux by 30–56%. The results of the study are practically significant for the development of an automated control system for BF-MBR, optimizing treatment rates together with membrane separation efficiency.

Keywords: biofilm membrane bioreactor; membrane fouling; coagulants; membrane flux enhancement; multivariate statistics; factorial experimental design

1. Introduction

Climate change, which is thought to be the reason for more frequent and intense droughts, results in dramatic environmental and economic consequences, entailing the losses of billions of euros [1]. As expected, this trend will continue to worsen, which, along with the gradually increasing population, will naturally deepen water stress in the European region [1]. According to estimations, by 2030, water stress and scarcity will potentially affect 50% of the river basins in Europe [2], which emphasizes the need for water reuse and the reduction of environmental impacts of wastewater treatment facilities.

Membrane bioreactor technology (MBR) is an advanced solution for water scarcity, which is gaining momentum worldwide. This tendency is mainly caused by drivers of the global MBR market such as stringent environmental legislation on wastewater discharge and reuse, water reuse advantages (resource and financial savings), beneficial application of decentralized wastewater management,

low footprint, easiness of automation, flexibility of the modular design, minimal requirements for daily supervision by the qualified staff, energy-cost efficiency and the decrease of membrane price [3–6].

However, membrane fouling deteriorates the membrane system's operation and remains a major bottleneck for MBR expansion. It is attributed to the deposition of biopolymers such as soluble microbial products (SMPs) and extracellular polymeric substances (EPSs) on the membrane surface and its pores [7–10].

Biofilm membrane bioreactor (BF-MBR) is an advanced innovation in the evolution of MBR technology, which allows reduction of membrane fouling to a certain extent and application of higher operational fluxes via the combination of a moving bed biofilm reactor (MBBR) and membrane bioreactor [11]. The MBBR part is based on the utilization of biofilm carriers at a high volumetric filling fraction (around 2/3 of the reactor volume), which are continuously suspended in the reactor by aeration [12]. Their introduction into the system minimizes the possibility of the occurrence of dead zones and creates a large contact area between the wastewater impurities and the active biomass.

According to the findings by Ivanovic and Leiknes [12], Ødegaard [13] and Phattaranawik and Leiknes [14], the biodegradation in BF-MBR is profoundly shifted towards the attached growth mechanism, which requires much lower concentrations of mixed liquor in the membrane separation part, entails lower fouling potential of mixed liquor, reduces the amount of the produced excess activated sludge and provides a resilient biological treatment.

Membrane fouling caused by the solids, colloidal matter and solutes remains a critical issue for BF-MBR, as is the case in MBR systems. The above-mentioned team indicated a higher content of the submicron particle size fraction in mixed liquor of the BF-MBR system [15], which was particularly apparent at high loading rates (high chemical oxygen demand (COD), short hydraulic retention time (HRT)) [16]. This effect is caused by a higher tendency of BF-MBR for floc breakage (deflocculation), induced by the biofilm carriers and intense aeration. It results in the production of the soluble microbial products and the particles of a diameter proportional to the membrane pore size, which tend to cause irreversible and irrecoverable membrane fouling [12,17–20].

The studies by Kulesha et al. [7] and Nouri et al. [21], reported high efficiency of chemical flux enhancement when applying inorganic coagulants in MBR, especially with regard to their flocculating ability. Therefore, application of inorganic coagulants is expected to be beneficial for the performance of the BF-MBR system, since they can aggregate fine particles generated in BF-MBR and hence, reduce permeability losses, thus contributing to steady membrane separation.

Since the attached growth part is decoupled from the MBR chamber and there is a minimum or zero demand on biomass recirculation in the BF-MBR system [3,22], the application of BF-MBR allows for using the chemical enhancement of the membrane filtration process with no concern about reducing biomass treatment potential.

Five primary mechanisms of fouling mitigation via coagulant/flocculant addition in MBR systems have been identified [7,23–25]: (1) enhancement of adsorption/charge neutralization, (2) the increase of relative hydrophobicity of the floccules, (3) the increase of the mean floccule size, (4) the reduction of the SMPs level in mixed liquor/decrease of supernatant organic concentration and (5) inhibition of gel layer formation and the reduction of specific cake layer resistance. However, the principal mechanisms and effects of coagulant action with respect to membrane fouling alleviation in the biofilm membrane bioreactor (BF-MBR) system are still unclear.

The following parameters of mixed liquor were found to be fundamental for the characterization of its fouling propensity and the mechanisms of fouling mitigation during chemical flux enhancement in MBR/BF-MBR: electrokinetic potential (ζ-potential), relative hydrophobicity (RH) of the flocs, the mean particle size or particle size distribution, chemical oxygen demand (COD) and mixed liquor suspended solids (MLSS) [15,16,26–28].

A successful application of Me-based coagulants for membrane fouling mitigation in MBR systems was admitted by different research groups [21,29–34]. Meanwhile, a limited number of studies can be found on chemical flux enhancement via coagulant addition in BF-MBR [22,35].

The prepolymerized aluminium coagulants have several advantages over non-prepolymerized Al- and Fe-based coagulants in the coagulation process; and likewise in membrane filtration systems—enhanced adsorption/charge neutralization potential, less alkalinity consumption (pH drop) for a given Me-dose, lower sensitivity to low temperatures and broader operational pH range [36,37]. Better performance of the prepolymerized aluminium chloride (PACl) in the MBR system was observed by Wu et al. [38] and Chen and Liu [39]. On the other hand, some research works reported a superior flux enhancement potential of non-prepolymerized Me-based coagulants in comparison to their prepolymerized counterparts [22,40]. The mechanisms behind the observed differences in coagulant performance are not well understood. There is a variety of PACl commercial products, with the variation in composition, depending on the supplier. It would be necessary to underline the governing mechanisms of membrane fouling mitigation by Me-based coagulants to select the optimum flux enhancer or compound basicity (in case PACl shows the highest fouling mitigation propensity).

The purpose of the current research is to present a viable concept of membrane fouling alleviation and optimization of membrane filtration based on a systematic comparative study of prepolymerized and non-prepolymerized inorganic coagulants, delving into the mechanisms of flux enhancement by applying chemometric analysis of the resulting membrane fouling mitigation patterns in the BF-MBR.

2. Materials and Methods

Prepolymerized aluminium coagulants have a highly specific nature and the characteristics of the commercial products vary with the supplier. On the other hand, the treated mixed liquor quality can vary depending on the feeding wastewater, system design and location of the facilities. Thus the optimum coagulation conditions for a particular mixed liquor system are case specific and need to be determined via the jar tests [41].

The following sequential strategy was developed to conduct a holistic assessment of the Al- and Fe-based coagulants as membrane flux enhancers for the BF-MBR system:

(1) the selection of the optimum pH at constant coagulant dosage for every tested coagulant during the jar tests;
(2) the jar tests, conducted at previously determined optimum pH for every coagulant, with the variation of the coagulant dose, to determine the relevant optimum dosage ranges;
(3) the total recycle test (TRT), with the pH correction and the application of the tested dosage ranges (depending on the coagulant), which exhibited promising results during the jar tests, to determine the optimum fouling mitigation conditions and the most efficient compound;
(4) the TRT without the pH correction, to assess the coagulant performance regarding fouling mitigation under the conditions, unfavourable for coagulation;
(5) partial least squares analysis using the data from the TRT, with and without pH correction, to study the effect of the selected mixed liquor characteristics on the fouling intensity after the chemical dosing and determine the principal mechanisms of coagulant action;
(6) the determination of the intrinsic coagulant charges and the qualitative analysis of the investigated prepolymerized aluminium coagulants regarding their molecular weight (MW) distribution;
(7) two-level factorial design of the experiment, applying the selected coagulant of the highest performance, to determine the optimum levels of factors for the maximum permeability/filtration time increase, discover the vital factors for the membrane flux enhancement and the tendencies in their interactions.

2.1. Study Object

Mixed Liquor (ML) for laboratory experiments was supplied by the aerobic BF-MBR pilot system, described in previous work by this team [42]. This decision was made to ensure high reproducibility and accuracy of results, which were intended to be further implemented at the mentioned pilot plant

facility and to have a source of representative mixed liquor, since the experimental laboratory setup, based on TRT, does not reproduce the biodegradation stage (MBBR) of the BF-MBR system.

The pilot system worked at solids retention time (SRT) 20 days, treating daily 0.3 m^3 of wastewater from the source-separated sewer network. The feeding inlet was the mixture of black to grey wastewater at the ratio 1:9 (MLSS 0.4–1.31 g/L, COD 142–262 mg-O_2/L, PO_4-P 6.08–10.28 ppm). Air was continuously supplied at the rate 60 L/min by the air compressor MEDO LA-60E (Nitto Kohki®, Nitto Kohki Co.,Ltd, Tokyo, Japan). Initial biological activity in the system was provided by inoculation with sludge from the municipal MBBR wastewater treatment plant (BEVAS, Oslo, Norway).

Four chemically different Al- and Fe-based membrane flux enhancers (MFEs) were selected for this study: non-prepolymerized aluminium and iron (III) sulphate and two prepolymerized aluminium coagulants with different basicity (Table 1). The applied coagulants are available from commercial suppliers by active compound name and metal content. Products of Kemira Chemicals AS (Helsinki, Finland) were used in this study.

Table 1. Properties of Membrane Flux Enhancers.

Designation	Active Compound	Metal Content, %	Basicity (OH/Me)	Density (20 °C), g/cm^3	pH
PAX18	[AlClOH]n	9.0 ± 0.2%	42.0 ± 2% (1.3)	1.37 ± 0.03	0.6
PAXXL61	$Al(OH)_xCl_{(3-x-2y)}(SiO_2)_y$	5.4 ± 0.3%	68.0 ± 5 % (1.9)	1.26 ± 0.03	2.7
ALS	$Al_2(SO_4)_3$	4.3 ± 0.1%	- (0)	1.33 ± 0.01	1.8
PIX313	$Fe_2(SO_4)_3$	11.6 ± 0.4%	- (0)	1.52 ± 0.06	<0.5

The correction of the pH values in mixed liquor before and during coagulation was performed with the aid of 0.01N NaOH in the case of aluminium coagulants and 0.1 N NaOH when applying iron (III) sulphate due to the higher tendency of the system for pH decrease in the latter case.

2.2. Jar Tests

After the selection of the proper chemicals, the adapted jar tests were used to simulate their application for the coagulation-flocculation in the separation chamber of the BF-MBR. The use of jar tests helped to accelerate and simplify the determination of the optimum conditions: pH and dosages. For this purpose, the Flocculator 2000 from Kemira Chemicals AS and 1 L beakers were used.

The following mixing conditions were applied during coagulation: 1 min rapid mixing (400 RPM), 10 min slow mixing (30 RPM), followed by 20 min of sedimentation with no mixing.

2.3. Total Recycle Test

The testing of a batch-type MBR in the total recycle mode for membrane fouling mitigation has been recently practiced in several studies [43–45]. It implies a continuous recycling of the whole permeate volume back to the membrane reactor during the experiment. The total recycle test (TRT) allows the experiment to maintain a stable content and volume of the coagulated mixed liquor during the filtration cycle, preventing the introduction of raw, untreated portions of mixed liquor into the system with already added flux enhancers, which could potentially cause high bias in the experiments. In the studies on the use of quorum sensing and quorum quenching to mitigate membrane fouling, TRT is also beneficial due to the maintaining of the effective concentration of the active enzyme throughout the system operation.

Prior to the filtration experiments, the integrity of the membrane sheets was evaluated through the bubble point test and the vacuum decay test via method F 316-03 (Reapproved 2011) and method D 6908-03, respectively, according to the American Society for Testing and Materials. Both tests are based on the determination of the diameter of the pore or defect calculated from its bubble point.

Total recycle tests (TRTs) were conducted in a plastic transparent 2.8 L MBR reactor, where the flat-sheet ceramic membrane was submerged with a provided cross-flow aeration (Figure 1).

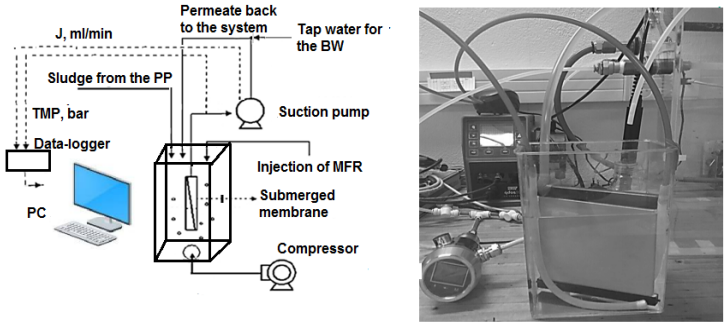

Figure 1. The total recycle test system, adapted from [43].

SiC microfiltration membrane sheets with 0.1 µm nominal pore size and surface areas of 0.0374 and 0.0355 m^2 were used for these studies (Cembrane, Lynge, Denmark). The vacuum was applied to the submerged membrane using a Qdos30 peristaltic metering pump. The separation process was carried out under constant flux conditions (80 LMH) with the recycling of all the filtrate to the source container. The pressure in the vacuum line was measured with an electronic pressure transducer (Klay 8000 series) and recorded into the laboratory data-logger. Recycling continued until the TMP reached a critical level of 1.2 times from TMP_{in} (initial transmembrane pressure) but not less than 1010 s. Filtration Time (F) was chosen as one of the fouling indicators during the membrane filtration experiments. Filtration time is the time required for reaching 1.2 × TMP_{in}. Coagulants were added to ML before membrane filtration and intensively mixed, applying aeration during 30 s. After this time, the aeration was turned off and the membrane system remained in the relaxation mode for 90 s more. Then, the aeration was turned on and the filtration started (Figure 2).

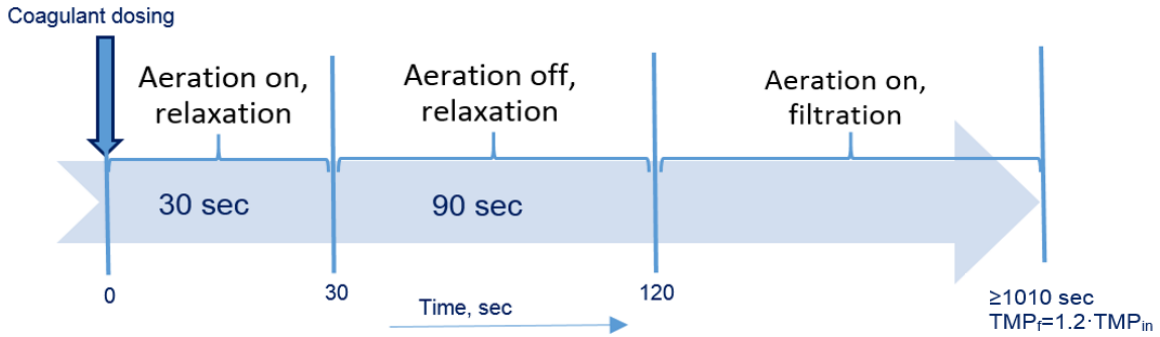

Figure 2. Experimental conditions of the total recycle test.

Ten minutes after the chemical dosing, the first sampling was performed in a quantity of 200 mL to keep the membrane fully submerged in the ML solution. 60 mL of this sample were used to measure MLSS, residual aluminium, PO_4-P and the particle size parameters. The rest of the ML was used for the measurement of electrokinetic potential and turbidity.

When TMP increased to the level of 1.2 × TMP_{in} and more than 1010 sec elapsed after the chemical dosing, the filtration was stopped and the specimens were taken.

Permeability was the other targeted fouling indicator, which was determined using the flux, normalized to 20 °C (Equation (1)).

$$P_N = \frac{J \cdot e^{(-0.032 \cdot (t-20))}}{TMP} \quad (1)$$

where J is a membrane flux, LMH; TMP is a transmembrane pressure, bar; t is an actual temperature of the experiment, °C.

The current research uses capillary suction time (CST) to express relative hydrophobicity. The negative correlation between them is demonstrated in the discussion section of this work.

At the end of filtration, mixed liquor was used for the measurement of capillary suction time (CST) and Time-to-Filter (TTF).

2.4. Applied Analytical Techniques

2.4.1. Mixed Liquor Analysis

Mixed liquor suspended solids (MLSS), capillary suction time (CST) and Time-to-Filter (TTF) were determined via the dry residue test 2540 D, CST test 2710 G and Time-to-Filter test 2710 H, respectively, according to SMWW (Standard Methods for the Examination of Water and Wastewater, 22nd edition).

Prior to the measurement of turbidity and zeta potential, the supernatant of the mixed liquor samples was filtered through the quantitative cellulose filter paper with the pore size 8–12 µm (Grade MN 640 md, Macherey-Nagel™, MACHEREY-NAGEL GmbH & Co. KG, Düren, Germany).

Electrokinetic potential (ζ-potential) was determined through the measurement of electrophoretic mobility and the automatic derivation of ζ-potential, according to Henry's equation under Zetasizer Nano-Z (Malvern™, Malvern Panalytical Ltd, Malvern, UK).

Turbidity was measured under HACH 2100 N IS Turbidimeter, according to ISO method 7027.

COD_{dis} was measured by the COD-cuvette test (HACH, Manchester, UK), applying the dichromate method, according to ISO 15705:2002 [46].

Orthophosphates (PO_4-P) and residual aluminium were measured using the EasyChem Plus colorimetric analyser (Systea™, Systea S.p.A., Anagni, Italy), in accordance with the automated colorimetric method, USEPA Method 365.1 and automated colorimetric Eriochrome Cyanine R method, respectively.

Determination of the particle size distribution was conducted in several steps. First, the acquisition of the images under a light microscope (Leica DM 6B) was performed with the camera Leica DMC4500 (90× magnification), which transmitted the images to the computer. For every image, the 2544 × 1816 pixel area was cropped by manual investigation of the area, followed by further image processing using ImageJ software [47] (Figure 3).

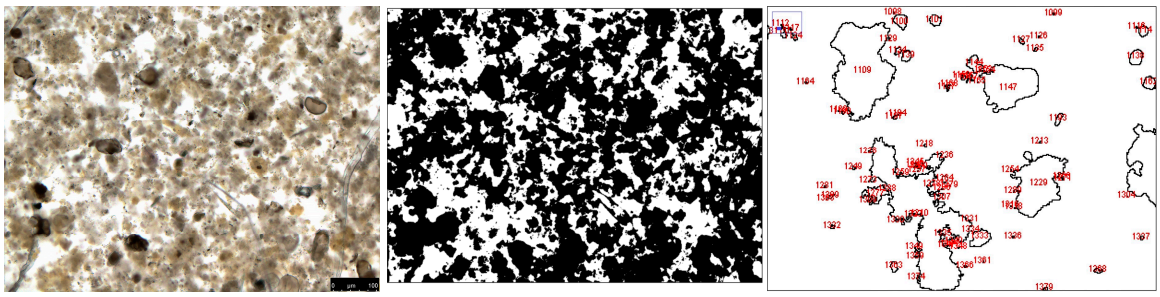

(**a**) (**b**) (**c**)

Figure 3. Determination of the particle size by image processing and analysis: (**a**) the original sample image, acquired under the light microscope; (**b**) the sample image after the adjusted threshold; (**c**) 200% magnified area in the image after particle analysis.

Then, the acquired particle areas were recalculated to the diameters, which were used as the basis for the cumulative distribution plot.

The determination of the particle size distribution (PSD) parameters, specified in Table S1 [48–52], helped to quantify and interpret the image analysis data.

2.4.2. Intrinsic Characteristics of the Coagulants

Potentiometric Titration

A streaming current detector (Micrometrix®, Micrometrix Corporation, Atlanta, Georgia, USA), connected to the automatic titrator (EasyPlus™, Mettler Toledo, Columbus, Ohio, USA), was used

for determination of the charges of the tested coagulants as well as for potentiometric titration of the mixed liquor samples.

For the coagulant charge determination, Potassium Polyvinyl Sulphate (PVSK) was used as a standard anionic polymer, while Methyl Glycol Chitosan (MGC)—as a standard cationic polymer. Both standard polymers were accurately prepared to the concentration 0.0005 N from the commercial colloidal titration solutions using 0.0025N PVSK and 0.005N MGC supplied by Wako® (FUJIFILM Wako Chemicals Europe GmbH, Neuss, Germany). PVSK was chosen to be a reference standard and MGC concentration was adjusted to equate to PVSK at pH 7. The ratio factor of polymers was determined at pH 7 and the working pH 1.86, 2.12, 2.3 and 2.7, which were selected according to the intrinsic pH values of the subsequently tested coagulants (Table 1).

Charges of the tested coagulants (1 mmol Me/L) were determined through the potentiometric back titration. At least two parallel measurements were conducted for every coagulant sample. The cationic charge concentration of every coagulant was calculated according to the following formula [53]:

$$Charge\ concentration = \frac{\left(\frac{V_{\mathrm{PVSK}} \cdot \mathrm{F} - \overline{V_{\mathrm{MGC}}}}{V_{aliquot}} \cdot 0.0005 \frac{equiv}{L} \cdot 10^6\right)}{m_{salt}/L}, \quad (2)$$

where *Charge concentration* is the determined concentration of the positively charged ions in the coagulant sample, μequivalent/mg_{salt}; m_{salt} is mass of the coagulant salt in 1 L, V_{PVSK} is the known added volume of PVSK, mL; F is correction factor; $\overline{V_{\mathrm{MGC}}}$ is the average volume of MGC, mL; 0.0005 is normality of the titrant standard equal to the gram equivalent weight of a solute per litre of solution equiv/L; $V_{aliquot}$ is the aliquot value of the titrated sample, mL.

Potentiometric direct titration of mixed liquor, applying investigated coagulants as titrants, was performed using the specimens, sampled on the same day for all the coagulants. The coagulants were applied as titrants with no dilution. A minimum of two parallel measurements were conducted for every coagulant.

Size Exclusion Chromatography

A total of 25 g of Bio-Gel P-100 Gel (Bio-Rad Laboratories™, Bio-Rad Laboratories, Hercules, California, USA) (medium polyacrylamide beads with wet bead size 90–180 μm, fractionation range 5000–100,000 MW) were suspended in 800 mL of distilled water and allowed to swell overnight. The swollen beads were put into a glass preparative chromatography column (Omnifit®, Diba Industries Inc., Danbury, CT, USA) (1.5 cm in diameter, 48 cm in length, working volume 78.6 mL), equipped with a PTFE/polyethylene frits, allowed to settle and washed with five bed volumes of the eluent–NaCl solution (0.5 mol/L, pH 2–2.7) until a constant height (44.5 cm) was obtained. 1 mL of the prepolymerized aluminium coagulant (PAXXL61 (2.52 mol Al/L) or PAX18 (4.57 mol Al/L)) were injected in the gel column and eluted at 0.7 mL/min, using an LC pump Perkin-Elmer Series 410 to control the elution rate. The fractions were further collected in the disposable sample cuvettes and assayed for total aluminium according to Eriochrome Cyanine R method [54] at appropriate points, using EasyChem Plus colorimetric analyser (Systea™, Systea S.p.A., Anagni, Italy).

For all separations, the same column was used. Before each experiment, gel was conditioned by at least 500 mL of the NaCl solution to wash out residual monomeric aluminium.

2.5. Statistical Mining of the Relationships in the System

In the current investigation, multivariate chemometric approach based on partial least squares analysis (PLS), that is, PLS-regression (PLSR), was applied to distinguish the relationships between the dose of the coagulant, the mixed liquor parameters and the fouling indicators during the Total Recycle Test.

PLS analysis is a multiple linear regression technique, which simultaneously models the matrices of the predictor variables and responses to find the hidden variables in X that will predict the

latent variables in Y. The creation of new predictor variables and responses, which are the weighted combinations of the raw variables, is accomplished through the following steps: (1) extraction of x-scores (t), that are the most correlated to Y; (2) generation of Y-loadings (q) from (t); (3) calculation of Y-scores (u) from (q); (4) plotting (t) and (u) together with the maximized covariance [55].

Due to the creation of the orthonormal weight loadings and the loadings, which are neither orthogonal nor normalized, PLS explains the maximum variance in the original data matrix X and meanwhile provides the maximum correlation between X and the vector of output variables y_n [56]. PLS analysis makes it possible to determine the independent influence of each input variable even if the analysed data is strongly collinear and noisy. Besides, PLS gives an opportunity to model a big number of X-variables with the simultaneous modelling of several response variables, Y [57,58].

The Unscrambler® X10.3 (CAMO Software AS, Oslo, Norway) was used to analyse the monitored data. Design-Expert® 10 software (Stat-Ease, Inc., Minneapolis, MN, USA) was used to build and analyse factorial experimental design.

3. Results

3.1. Jar Tests

Coagulant efficiency highly depends on the pH of the solution. It is the most critical parameter since it determines the charge of the colloidal impurities and the dominance of certain competitive hydrolysis reactions and hence, the nature of polymeric hydrolysis species [59–61]. According to Ratnaweera [60], the hydrolysis reaction is much faster than the pH correction procedure, using the typical laboratory equipment, which results in the discrepancy between the measured pH after coagulation and the actual pH of the hydrolysis. Hence, it was decided to adjust the pH of the mixed liquor solution mainly before the coagulant dosing. However, the pH adjustment during the coagulation process was also included when the pH decreases during coagulation exceeded 0.5 units.

It was decided to test a different down limit of pH values for PIX313 in comparison to that of the aluminium coagulants, taking into consideration the following findings by Stumm and Morgan [61], further developed by Bratby [59]:

(1) The ligands, which are representative of ionogenic functional groups and characteristic of the hydrophilic colloids (proteins, polysaccharides and humic substances), such as phosphate, pyrophosphate, oxalate, salicylate (with a carboxyl and an aromatic hydroxyl group), show the tendency to displace the H_2O groups in aquo-metal ions of the coagulant, which satisfies the coordinative requirements of Fe(III) and Al(III), which results in the formation of the Me-ligand complexes;

(2) OH^- ions have a stronger affinity for the Fe^{3+} and Al^{3+} than other ligands, including the representative of functional groups of colloids; however, the latter may compete with OH^- for the coordinative sites;

(3) When the ratio ligand/OH^- increases, which can be reached by pH decrease in the system, ligands, which originate from the functional groups, may partially or entirely substitute for OH^- in the charge neutralization of the metal cations;

(4) Fe^{3+} has a higher affinity for OH^- than Al^{3+}; thus, lower pH is required for the formation of ionized function group-Me complexes to limit the statistical opportunity of the complexation of OH^-.

The application of lower pH values for the iron (III) coagulant can also be justified by the diagrams with equilibrium-solubility domains concerning $Fe(OH)_3$ and $Al(OH)_3$ in water as a result of hydrolysis of $Fe(H_2O)_6^{3+}$ and $Al(H_2O)_6^{3+}$, which were introduced by Stumm and O'Melia [62]. According to the diagrams, the iron (III) hydroxo- and polyhydroxy complexes form at lower pH values and wider pH range compared to their aluminium-based counterparts. As specified by Meyn et al. [63], iron (III) complexes, formed at a lower pH, provide higher removal of organic matter, than those which occur at a higher pH.

It is worth noting that, according to Liang et al. [64], the presence of sulphate ion in the skeleton of coagulants shifts their applicable coagulation pH towards the acidic regions, which enables efficient coagulation-flocculation at lower pH than for the species with chloride or nitrate ions in the coordination sphere.

The determination of the optimum pH for the applied coagulants, using the mixed liquor samples, was further conducted (Figure 4). The coagulant dosage is expressed by mixed liquor concentration as µmol Me per mg of suspended solids (SS). It was decided to apply lower dosages: 0.4 µmolAl/mgSS of aluminium-based coagulants and 0.9 µmolFe/mgSS of iron (III) sulphate, which would not sharply reduce pH of the solution, consequently, to avoid adding excessive amounts of NaOH and to simplify the maintenance of the desired pH values.

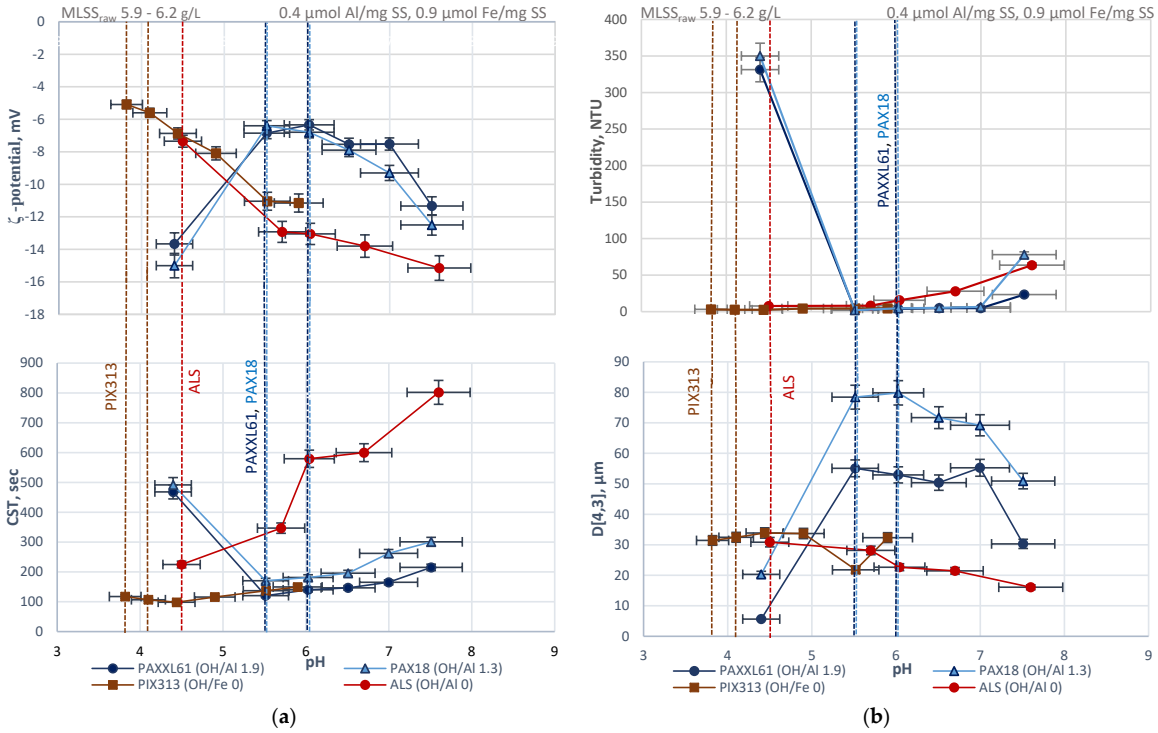

Figure 4. Determination of the optimum pH at fixed coagulant dose during the jar tests according to: (**a**) zeta potential, capillary suction time (CST); (**b**) turbidity, the volume moment mean.

Zeta potential profiles demonstrate the nature and intensity of electrostatic interactions between the flux enhancing additives and the negatively charged foulants in the system [65].

Zeta potential (ζ-potential) is the electrokinetic potential at the slip plane between the Stern Layer and the diffuse layer, which is related to the electrophoretic mobility of the particle, according to the Henry equation and is one of the main double layer characteristics in the charged colloid. Zeta potential characterizes the resistance of the colloidal system to aggregation and provides a quantification of the double layer capacity.

If $|\zeta| \geq 30.0$ mV, the disperse system is sufficiently stable and no coagulation is observed. According to the classification, introduced by American Water College [66], the average zeta potential equal to −20.0–(−11.0) mV refers to poor coagulation degree, −10.0–(−5.0) mV to fair coagulation degree, −4.0–(−1.0) mV to excellent coagulation degree and 0.0–3.0 mV refers to maximum coagulation degree.

According to the represented profiles (Figure 4), the maintenance of pH at 5.5–6.0 during the application of the prepolymerized aluminium coagulants, characterized by high and medium basicity, provided the maximum degree of destabilization of the mixed liquor suspension at the selected dosage. At pH 5.5–6, zeta potential values for PAXXL61 and PAX18 were in the range: −6.9– (−6.3) mV and

−6.8–(−6.4) mV, respectively, resulting in the lowest residual turbidity among the tested pH values: 2.5–3.9 NTU and 2.0 and 4.6 NTU, respectively, which indicates the highest coagulation efficiency under the applied conditions. According to the CST plots, pH values 5.5–6.0 also favoured the highest mixed liquor dewaterability and, hence, the highest relative hydrophobicity of the flocs in this set of experiments. The results on the volume moment mean particle size showed that the defined pH range for the prepolymerized aluminium coagulants provided the maximum sizes of the floccules: 53.0–55.0 µm and 78.0–79.8 µm for PAXXL61 and PAX18, respectively.

Meanwhile, the optimum pH values for non-prepolymerized aluminium and iron (III) coagulants were found to be lower than for the prepolymerized aluminium coagulants; they were equal to 4.5 and 3.8–4.1, respectively. The defined pH values for ALS and PIX313 provided the maximum absolute zeta potential levels: −7.4 mV and −5.6–(−5.1) mV, respectively; high extent of dewaterability—225.0 s and 107.0–117.5 s, respectively; and relatively large volume moment mean particle size—30.9 µm and 31.4–32.5 µm, respectively, in comparison to the other tested pH values under the maintained conditions.

More detailed data is provided in Table S2.

The required pH around 3.8–4.1 for iron (III) sulphate coagulant, which is more acidic than for the aluminium coagulant, is consistent with the findings by other studies [63,67].

To sum up, the determined optimum pH values foster the enhancement of adsorption/charge neutralization, the increase of relative hydrophobicity of the flocs and the increase of the particle size, which are assumed to be representative indicators of the fouling potential of mixed liquor, whose characteristics are modified with the coagulants.

The next stage was the determination of the optimum coagulant dose, maintaining the established levels of the optimum pH in the system. The obtained results of the relevant jar tests are represented in Figure 5.

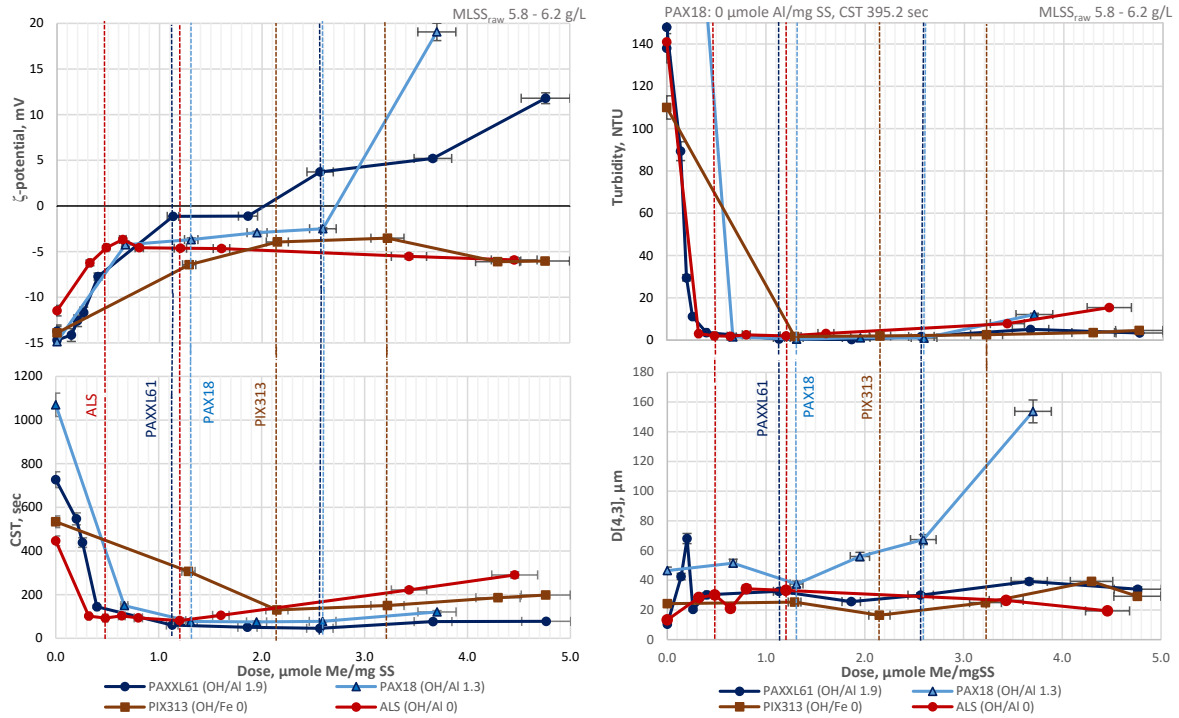

Figure 5. Influence of the coagulant dose on the monitored parameters at fixed pH during the jar tests: (**a**) zeta potential, capillary suction time (CST); (**b**) turbidity, the volume moment mean.

Jar tests allowed the team to determine the dosage conditions that promoted the maximum increase of relative hydrophobicity of the flocs, the reduction of the absolute zeta potential value, the

decrease of turbidity and the increase of the mean particle size (expressed through the volume moment mean), which is summarized in Table S3.

The acquired zeta potential profiles (Figure 5a) demonstrate that merely prepolymerized aluminium coagulants provided complete neutralization of mixed liquor, which indicates their higher charges in comparison to their non-prepolymerized counterparts. Both PAXXL61 and PAX18 assured the maximum coagulation degree (0.0–3.0 mV). It is worth noting that high neutralization potential of prepolymerized aluminium coagulants can result in their tendency to overcompensate the particle charges with the subsequent recharging of the system (ζ-potential = 5.0 mV or higher) and its restabilisation, which is observed at the dosages higher than 4.8 μmolAl/mgSS for PAXXL61 and 3.7 μmolAl/mgSS for PAX18. System restabilisation is undesirable since it worsens flocculation of the particles, deteriorates the treatment efficiency, entails additional costs of reagents and can have a detrimental effect on the aquatic fauna after wastewater discharge due to the risk of high residual aluminium concentrations [68,69].

Therefore, a defined range of optimum dosages should be further applied.

According to the results (Figure 5a) for non-prepolymerized aluminium and iron (III) sulphate coagulants, zeta potential remains negative over the whole dosage range. Neither of the non-prepolymerized coagulants was able to reach the maximum degree of coagulation (0.0–3.0 mV) but attained rather fair (−10.0–(−5.0) mV) and in single cases—excellent (−4.0–(−1.0) mV) degree, which is an indicator of weaker charge neutralization capacity possessed by these coagulants. As assumed by Gregory and Duan [37], the coagulation in this region of zeta potential values occurs entirely via the adsorption of suspended matter on the precipitated $Al(OH)_3$.

Meanwhile, the obtained plots demonstrate, that the overdosing of ALS and PIX313 can still cause the deterioration of the mixed liquor system, which is observed by the elevated levels of turbidity, CST and the decrease of the volume moment mean particle size, which is clearly observed at 3.4–4.5 μmolAl/mgSS and 4.8 μmolFe/mgSS.

All of the investigated coagulants are highly efficient with respect to colloidal matter removal, which is indicated by low values of the final turbidity—0.5–2.6 NTU (Figure 5b). Hence, good coagulation performance is achieved for every coagulant in the defined optimum dosage regions.

The character of the CST graphs points out that the studied coagulants highly reduce the affinity of the mixed liquor particles for water, thus increasing their hydrophobicity, the ability to aggregate and settle [70,71] and decreasing their potential to attach to the hydrophilic membrane surface.

Particle size analysis (Figure 5b) demonstrates that the prepolymerized aluminium chloride with medium basicity PAX18 exhibited the greatest flocculation ability among all studied coagulants, which was particularly apparent in the range of dosages 2.0–3.7 μmolAl/mgSS, when the volume moment mean, D[4,3], reached 56.0–153.7 μm. The second-highest particle size 42.0–68.0 μm was attained, applying prepolymerized aluminium chloride with high basicity PAXXL61. However, its increase with the dosage was not as continuous as in the case of its counterpart with lower basicity and is characteristic merely for the narrow range of dosages 0.1–0.2 μmolAl/mgSS. Concerning non-prepolymerized inorganic coagulants, their flocculating efficiency was not so pronounced, since the particle sizes underwent merely minor changes. Better performance of prepolymerized aluminium coagulants can be explained by their higher charge, which results in enhanced adsorption-charge neutralization of the mixed liquor particles [36,38] and higher sensitivity of the Al hydrolysis species, which originated from the non-prepolymerized coagulants, to mixing conditions [72].

According to Figure 5, prepolymerized aluminium coagulants exhibit fairly broad ranges of optimum dosages in comparison to the non-prepolymerized coagulants, which agrees with the previous findings [36].

As a result, optimum pH values and the optimum coagulant dosages were determined and established as the point of reference for the subsequently conducted total recycle test.

3.2. Total Recycle Test

According to the assessment of the integrity of the membrane sheets, the minimum diameter of the defects on the membrane surfaces ranged from 10.2 to 17.0 µm. Those sheets, characterized by a significant difference between the openings in the membranes (Δ_{max} = 5.5 µm), were excluded from further experiments in order to eliminate the membrane factor from the potential influences affecting the difference in fouling intensity during the experiments.

The TRT was used to estimate the coagulant performance in the BF-MBR system and to validate the selected fouling indicators as regards their ability to demonstrate the fouling propensity of mixed liquor.

For every sample, the average normalized permeability values were calculated as follows:

$$avP_N = \overline{\overline{P^{in}_{N\,n}}; \overline{P^{fin}_{N\,m}}}, \quad (3)$$

where N is the number of values taken into consideration, N = 10; $\overline{P^{in}_{N\,n}}$ is the mean of the first ten values (n ≈ 210–400 s from the beginning of the filtration) of the normalized permeability, excluding the ramp of the peristaltic pump; $\overline{P^{fin}_{N\,m}}$ is the mean of the ten final values (m ≈ 790–1010 s from the beginning of the filtration) of the normalized permeability at the end of the filtration cycle.

For this purpose, a steep phase of the normalized permeability (P_N) development over time was chosen, followed by the calculation of the average normalized permeability (avP_N) within the range, that covered the initial rapid flux decline stage—seconds no. 210–1010 (Figure 6a). The selected array of values is related to conditioning fouling, which is characterized by pore blocking and adsorption of the SMPs on the membrane [73].

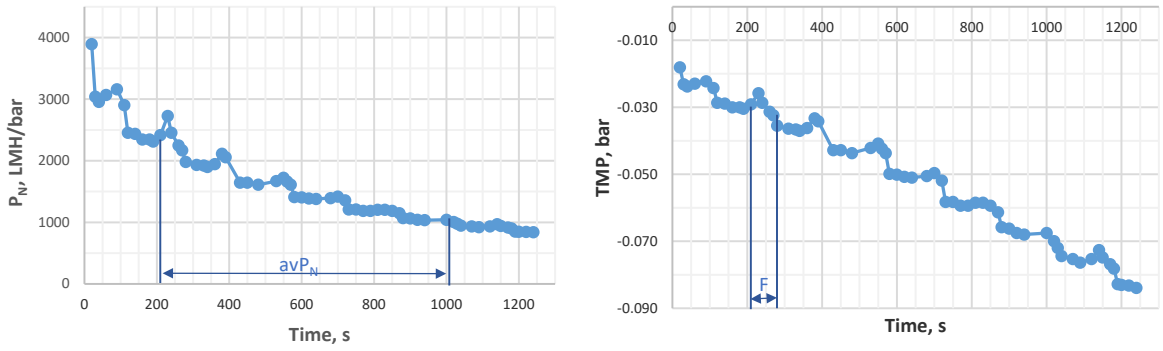

(**a**) (**b**)

Figure 6. Average normalized permeability (**a**) and filtration time (**b**), determined from the total recycle test.

Filtration Time (FT) was calculated from the logged TMP = f(time) (Figure 6b).

The steep development of the trend TMP = f(time) in Figure 6b can be explained by the fact, that the graph represents the data of the raw sludge filtration, characterized by a rapid TMP increase. It is worth noting that the constant flux of the filtration during all the experiments equal to 80 LMH lies in the critical flux region, which was intentionally selected after the critical flux experiments, using raw mixed liquor, based on the flux-step method [74], to estimate the coagulant performance in subsequent experiments under conditions unfavourable for membrane filtration.

Optimum pH values and dosage ranges, determined during the jar tests (Tables S2 and S3), were applied during the total recycle tests. The obtained results, related to the monitoring of the traditional parameters of wastewater treatment quality, are demonstrated in Figure 7.

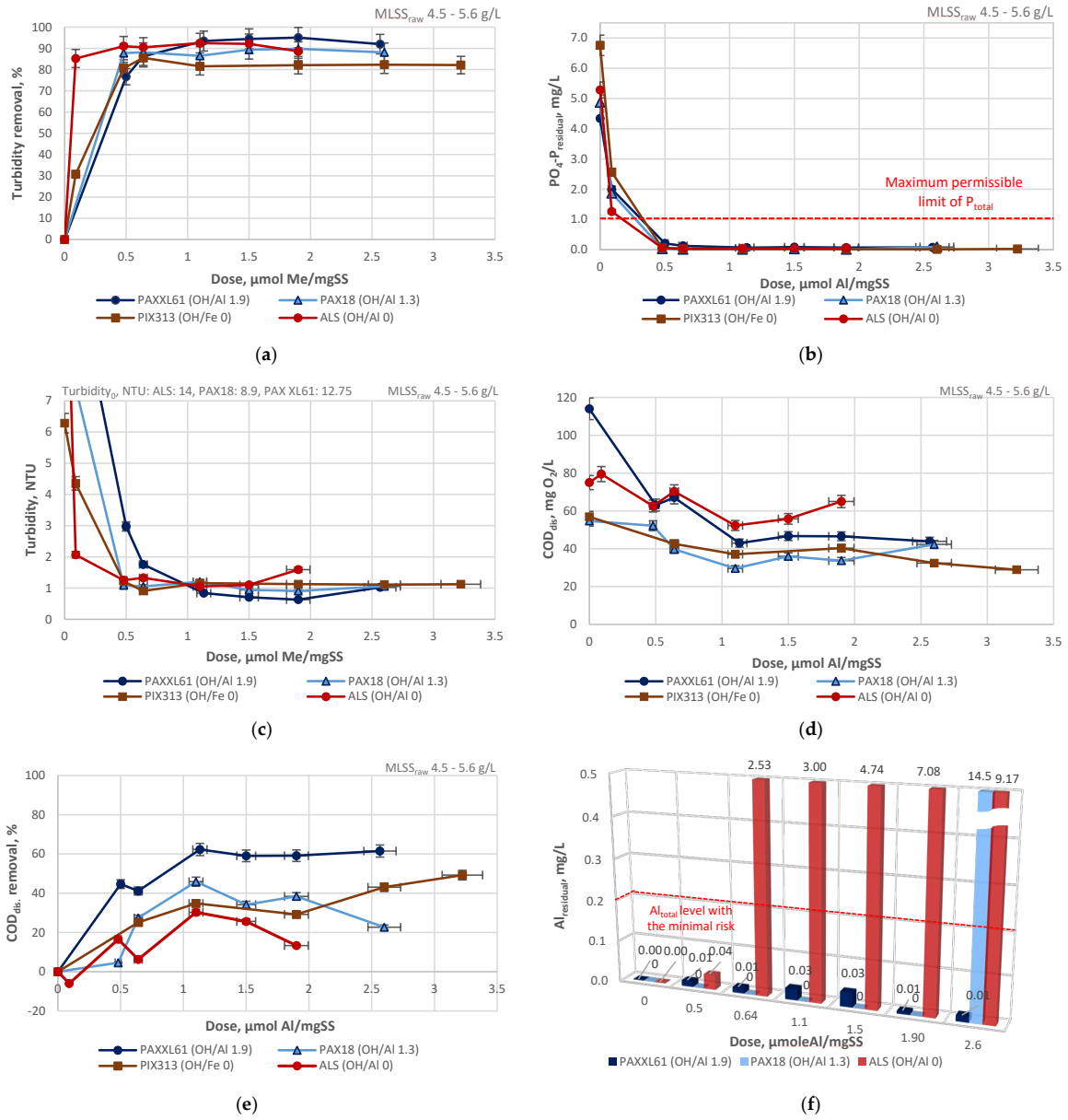

Figure 7. Influence of the coagulant dose on the parameters of treatment efficiency at fixed pH during the total recycle test (TRT): (**a**) turbidity removal; (**b**) residual orthophosphates; (**c**) turbidity, (**d**) dissolved COD (COD_{dis}); (**e**) COD_{dis} removal; (**f**) residual aluminium.

As shown in the graphs (Figure 7a,b), at 0.6 µmole Me/mgSS all the coagulants provide high effluent quality with respect to turbidity removal and residual orthophosphate concentration: 85.5–90.5% and 0.01–0.13 mg P-PO_4/L, respectively. The maximum permissible limit for total Phosphorus in the effluent of WWTP is 1.0 mg P_{total}/L [75]. Hence, all the coagulants provide the effluent quality in compliance with the regulations. The high potential for orthophosphate removal, exhibited by both prepolymerized and non-prepolymerized coagulants at the selected dosage ranges, agrees with the results acquired by Ødegaard et al. [36] and Ratnaweera et al. [76].

According to the turbidity removal plot (Figure 7a), the coagulant with high basicity PAXXL61 provides the highest performance, which agrees with previous works [76].

The comparison of turbidity and COD_{dis} profiles (Figure 7c,d) shows that the restabilisation in the samples applying PAX18 and ALS, which occurs at the dosage 2.6 and 1.9 µmolAl/mgSS, respectively, is equally pronounced in the COD_{dis} and turbidity analysis. This observation indicates that the colloidal particles $\leq$ 0.45 µm were not transferred to the higher size fraction $\geq$ 1 µm at

overdosing. In contrast, in the case of PAXXL61, lower residual COD concentration is observed at the overdosing (2.6 μmolAl/mgSS), even though the turbidity profile shows the tendency to increase, which apparently is an indicator that PAXXL61 (the coagulant with the highest tested basicity) is responsible for the enlargement of the fine colloidal particles to the size ≥ 1 μm at high dosages.

The increase of residual COD_{dis} in the overdosing region for PAX18 could be the result of floc breakage or the formation of some Al-organic complexes and for ALS, probably the Al-organic complex formation, which corresponds to the findings by Zhang et al. [77].

PIX 313 demonstrated, similar to PAXXL61, behaviour in the overdosing region but with a lower treatment efficiency with regard to the removal of COD_{dis} and turbidity. At 5.2 μmol Fe/mgSS (not shown on the graphs) the COD_{dis} removal (δCOD_{dis}) increased to 51%, while the residual turbidity increased by 23% in comparison to the relevant values at the dosage 3.2 μmol Fe/mgSS, which suggests an improved flocculation of the fine colloids (≤ 0.45 μm).

The maximum COD_{dis} removal in the dosage range 0.6–1.9 μmol Me/mgSS, was observed for both prepolymerized aluminium coagulants, PAXXL61 and PAX18, being in the range 41–62% and 27–46%, respectively (Figure 7e).

The data-driven sample grouping was manually performed for the dosage range 0.5–3.2 μmol Me/mgSS by dividing the band of the δCOD_{dis} values (Figure 7e) in the whole range between the upper and lower limits into three groups. As a result, the following ranges were generated: −51.0–17.0%; 17.0–27.0% and 27.0–62.3%. The range with the highest level of COD_{dis} removal (27.0–62.3%) was chosen as the target level. This selection agreed with the following mechanism of fouling control: the reduction of the SMPs level in mixed liquor. Consequently, the ranking trend among the studied coagulants in decreasing order of dominance of SMP removal mechanism, can be classified as: PAXXL61 (100% of all PAXXL61 samples) > PAX18 (67.0%) = PIX313 (67.0%) > ALS (20.0%), which corresponds to the findings in the previous works [30,36,60].

In the BF-MBR pilot system, COD removal due to biodegradation was in the range 67.0–92.0%.

According to the residual aluminium plot (Figure 7f), the application of prepolymerized aluminium coagulants is the most preferable, since in the range 0.5–1.9 μmol Al/mgSS they provided the concentrations of soluble Al at the level 0–0.03 mg Al/L, which is well below the regulatory limits [54,78–80]. Meanwhile, in the case of overdosing of PAX18, its residual aluminium concentration drastically increased up to 14.5 mg Al/L, which was almost 15 times higher than its content in the optimum coagulation region. On the contrary, ALS is characterized by incredibly high residual aluminium levels (starting from the dosage 0.64 μmol Al/L), which are in the range 2.5–9.2 mg Al/L. Consequently, the use of PAX18 in the overdosing region, as well as ALS at the dosages, higher than 0.5 μmol Al/mgSS, is undesirable from the environmental point of view.

The other monitored characteristics of mixed liquor, obtained during the TRT with the pH maintenance, are represented in Figure 8.

The zeta potential plot (Figure 8a) demonstrates that in the range 0.6–1.9 μmol Me/mgSS all of the coagulants provided an "excellent/maximum" coagulation degree, which indicates the achievement of their full charge neutralization potential under the applied conditions. As in the case of jar tests (Figure 5a), the prepolymerized aluminium chloride with medium basicity showed a tendency toward overdosing at a lower dosage than its counterpart with a high OH/Al ratio. Apparently, this is the result of the higher adsorption/charge neutralization potential of PAX18 in comparison to PAXXL61, which should be a subject of further investigation. The overdosing of PAX18 is characterized by severe system recharge, which is demonstrated by the zeta potential plot (Figure 8a), when zeta potential exceeds +18 mV, indicating system restabilisation.

TTF change profiles (Figure 8b) demonstrated a strong advantageous effect of PAXXL61 and ALS on the mixed liquor filterability, since they provided the maximum decrease of the filtering time (time to obtain 100 mL of the filtrate by TTF) by 79.5% and 85.0%, respectively. Meanwhile, PAX18 and PIX313 exhibited a less pronounced performance in affecting the mixed liquor filterability—the maximum TTF reductions were 59.5% and 63.0%, respectively. The acquired profiles (Figure 8b) also

show an increasing tendency of time-to-filter in the overdosing region for every one of the coagulants, which, in practice, can result in the decrease of mixed liquor quality and the deterioration of the membrane filtration process.

CST change graphs (Figure 8c) indicate the highest efficiency of PAXXL61 among the tested coagulants in terms of CST decrease and hence, the increase of relative hydrophobicity of the flocs. PAXXL61 provided a CST reduction equal to 61.0%, while the samples treated with PIX 313, PAX18 and ALS, were characterized by less significant CST alterations—34.0%, 25.0% and 24.6% CST reductions, respectively. Thus, it can be concluded that the coagulant with the highest tested basicity, PAXXL61, exhibited the highest performance with regard to the increase of relative hydrophobicity of the microbial floccules.

According to the plot of volume moment mean change (Figure 8d), the average particle size of the coagulated samples decreases in the following order of applied chemicals: PAX18 > PAXXL61 > PIX313 > ALS. This observation, together with the results of the prior jar tests (Figure 5b), suggests the dominance of the flocculating ability of the prepolymerized aluminium chloride with medium basicity over the other tested coagulants.

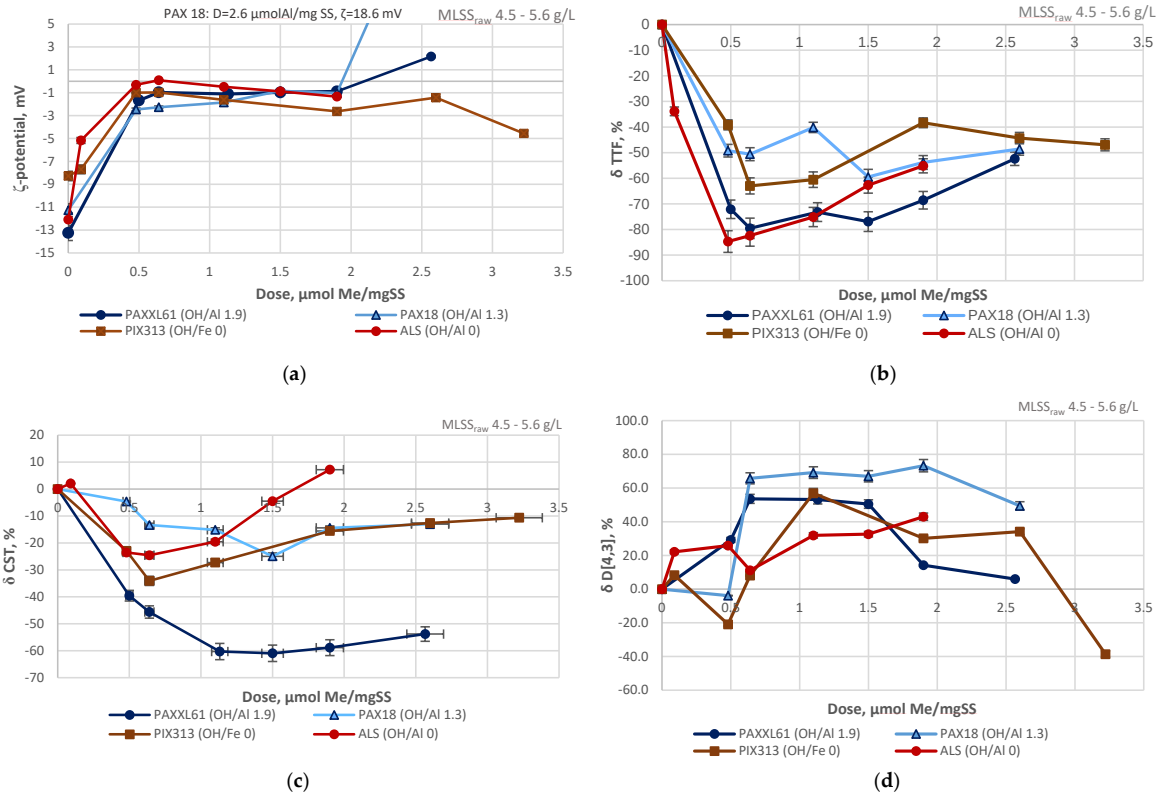

Figure 8. Influence of the coagulant dose on the monitored parameters at fixed pH during the total recycle test (TRT): (**a**) zeta potential; (**b**) TRT change; (**c**) CST change; (**d**) volume moment mean change.

The filtration time, required for reaching 1.2 × TMP_{in} and the average normalized permeability were chosen as the indicators of membrane fouling intensity. The acquired tendencies depending on the coagulant type and dosage, which were observed during the TRT at the fixed pH, are demonstrated in Figure 9.

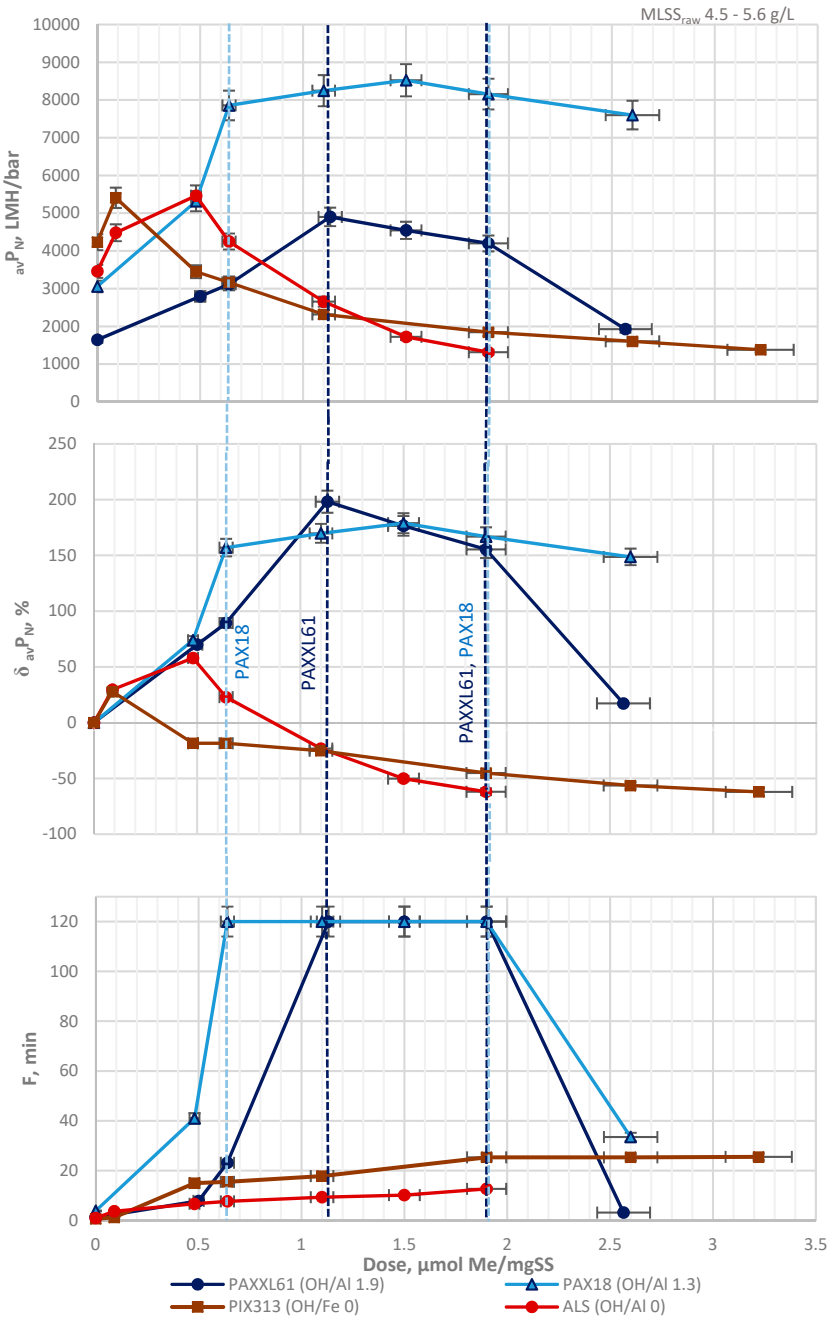

Figure 9. Relationship between the coagulant dose and the filtration performance according to normalized permeability, normalized permeability change and filtration time at fixed pH during the TRT.

According to Figure 9, the prepolymerized aluminium coagulants provided the greatest extent of fouling inhibition among the studied compounds: the maximum filtration time (F) equal to 120 min and the maximum increase of average normalized permeability ($\delta_{av}P_N$) by 155.0–198.0%.

According to the calculations for the BF-MBR pilot system, the obtained prolongation of the filtration times in the dosage range 0.6–1.9 µmol Al/mgSS for PAX18 or 1.1–1.9 µmol Al/mgSS for PAXXL61 (Figure 9) results in a tenfold increase in filtration time of the membrane separation cycle and 30.0–56.0% higher net flux (depending on the operational period), in comparison to the net flux in this system without the PACl dosing. Inhibited fouling intensity requires lower frequencies of the physical cleaning procedures (backwash and relaxation). Consequently, the addition of the studied

prepolymerized aluminium coagulants will highly improve the filtration efficiency of the BF-MBR pilot system.

Nevertheless, the coagulant with medium basicity, PAX18, demonstrated a superior fouling mitigation behaviour to PAXXL61, the prepolymerized aluminium chloride with high OH/Al ratio, since PAX18 has a higher flux enhancing efficiency at lower dosages and a wider range of maximum performance than PAXXL61 (Figure 9). The highest efficiencies of PAX18 during the filtration experiments is predominantly attributed to a greater adsorption/charge neutralization potential of PAX18 over PAXXL61, with subsequent flocculation enhancement, which was indicated by the relevant zeta potential and the mean particle size profiles.

The results of the total recycle test, conducted at the selected pH values, are summarized in Table S4.

Since PAX18 has a broader range of optimum dosages and a lower dose is required to reach the region with maximum values of the response functions, it was decided to apply this coagulant in the further stages of the research.

3.3. TRT with pH Control vs. TRT with Non-Corrected pH

The examination of fouling mitigation efficiencies of the selected coagulants during the total recycle tests without the pH adjustment was performed to estimate if it was reasonable to omit the pH adjustment stage. Such a decision was taken due to the fact that most conventional chemical wastewater treatment plants operate with no pH maintenance. In this case, the pH of the hydrolysis in mixed liquor depends on the characteristics of applied coagulants (acidic properties and the dosage) and the buffering capacity of mixed liquor [36]. The results are demonstrated in Table S5.

The results in Table S5 indicate that the pH of coagulation without the pH correction was the lowest for non-prepolymerized coagulants. Along with the intensive hydrolysis processes, the reason for the drastic pH decrease in the system could be the acidic properties of hydrated iron and aluminium ions, since they belong to Lewis acids, that is, proton donors, which transfer a proton to a solvent water molecule (Equation (4)).

$$\begin{aligned} Fe(H_2O)_6{}^{3+} + H_2O \leftrightarrow [Fe(H_2O)_5OH]^{2+} + H_3O; \\ Al(H_2O)_6{}^{3+} + H_2O \leftrightarrow [Al(H_2O)_5OH]^{2+} + H_3O. \end{aligned} \quad (4)$$

Moreover, the base-10 logarithm of a first acid dissociation constant (pK_a) for $[Al(H_2O)_6]^{3+}$ is higher than for $[Fe(H_2O)_6]^{3+}$, indicating lower acidity of hexa-aquo-aluminium complexes than hexa-aquo-iron complexes [61]. Hexa-aquo-aluminium complexes tend to decrease the pH of solution less dramatically, than their iron-based counterparts.

According to the obtained results (Table S5), PAXXL61, PAX18 and ALS provide much higher fouling mitigation efficiencies during the TRT, with the controlled pH, than without its maintenance. PIX313 also demonstrates positive tendencies with regard to improvement of membrane filtration. However, for PIX313 during the TRT at fixed pH, the normalized permeability started to decline at the dose 0.5 µmol Fe/mgSS, while the fouling rate continued to decrease. The potential reason could be the tendency of iron (III) coagulant at certain concentrations to trigger the formation of the Fe-rich gel matrix of polysaccharides on the membrane surface, thus increasing reversible fouling, which was reported by several studies [8,81,82].

In addition to high improvement of membrane filtration with the pH adjustment, the optimum filtration parameters are reached at lower dosages in comparison to those obtained during TRT with no pH correction. Lower coagulant dosages result in lower excess sludge production. Consequently, pH adjustment is a valuable tool in the optimization of the fouling mitigation based on coagulant dosing.

3.4. Investigation of the Characteristics of the Coagulants

The investigation of the coagulant characteristics was performed in order to describe the mechanism of charge neutralization and the extent of its prevalence depending on the coagulant nature. The results could potentially shed some light on the reason the coagulant with medium basicity, PAX18, performs more efficiently in respect of fouling mitigation than PAXXL61, of high basicity, whose potential to adsorption/charge neutralization was expected to be higher.

3.4.1. Coagulant Charges

The results of potentiometric back titration of the investigated coagulants are represented in Figure 10.

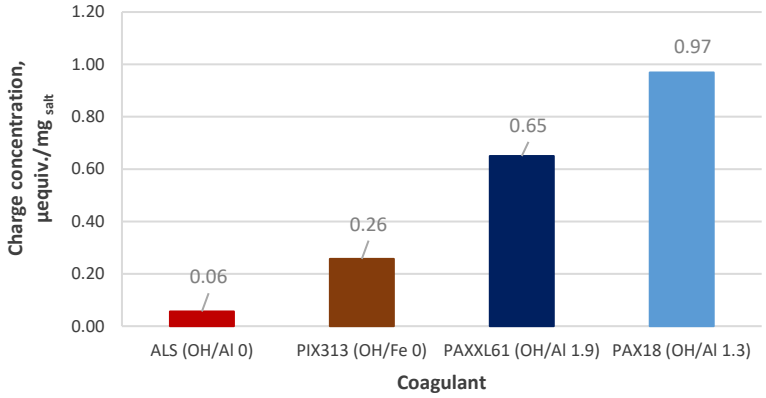

Figure 10. Charge concentrations of the studied coagulants.

According to the acquired charts (Figure 10), PAX18 and PAXXL61 have the highest charge concentrations, which correspond to their high efficiency regarding the increase in average normalized permeability and filtration time (Figure 9). Nevertheless, the charge concentration of PAX18 is still higher (0.97 μequiv./mg_{salt}) than the charge concentration of PAXXL61 (0.65 μequiv./mg_{salt}), which could be caused by the fact that, except for high basicity, PAXXL61 is characterized by the incorporation of SiO_2 group in its skeleton. As calculated by the authors of the current paper, based on the patents for similar commercial products [83,84], PAXXL61 has the approximate ratio of Al/Si of 15–20. The introduction of SiO_2 into the prepolymerized aluminium structure increases the molecular weight (MW) of the coagulant, and, due to the neutrality of silica group, decrements the coagulant charge concentration, which corresponds to the discoveries by Zouboulis et al. [85] and Gao et al. [86]. Besides, the interaction of Al with the polysilicic acid during the formation of polyaluminium silicate chloride species results in the creation of chelate-like bonding between the aluminium atoms and the polysilicic acid, which entails the hindering of the active polymeric $Al_{13}O_4(OH)^{7+}{}_{24}$ component formation during the subsequent prepolymerization phase. As a result, the content of monomeric octahedral Al_1 species in the final product increases, which reduces its adsorption/charge neutralization potential [87,88].

The charge concentrations of the non-prepolymerized coagulants, PIX313 and ALS were found to be much lower and were equal to 0.26 and 0.06 μequiv./mg_{salt}, respectively. Thus, non-prepolymerized coagulants tend to have lower charge concentration and less potential to enhance adsorption/charge neutralization than their prepolymerized counterparts, which confirms the findings of the previous studies [36].

In order to confirm the strength of investigated coagulants with respect to adsorption/charge neutralization, a series of experiments, based on direct potentiometric titration of the mixed liquor samples, was conducted (Figure 11).

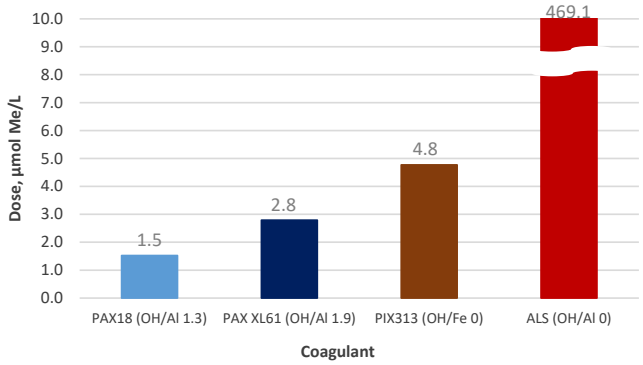

Figure 11. Coagulant dose required for reaching the endpoint during the potentiometric titration of mixed liquor.

According to the obtained results (Figure 11), the application of PAX18 produces the effect of reaching the titration endpoint at the lowest dose of 1.5 µmol Al/L. This, together with the acquired zeta potential profiles (Figures 5a and 8a) and the determined coagulant charges, is strong evidence for the highest potential to adsorption/charge neutralization of the coagulant with medium basicity, PAX18, among all the coagulants, studied in this research.

In addition to the determination of coagulant properties, the implementation of the potentiometric titration of mixed liquor with investigated coagulants, based on the streaming current detection, demonstrates that this system can be readily scaled up to perform the coagulant dosing and its online control at industrial BF-MBR. This conclusion refers to the fact that streaming current detectors are commercially available and appear to be among the key solutions to online control of coagulant dosing at wastewater treatment plants [89,90].

3.4.2. Chromatographic Separation of Prepolymerized Aluminium Coagulants

The comparative qualitative analysis of the investigated prepolymerized aluminium coagulants as regards their molecular weight (MW) distribution was performed using size exclusion chromatography. Figure 12 shows the MW distributions of the aluminium species in the samples of the prepolymerized aluminium coagulants of medium and high basicity.

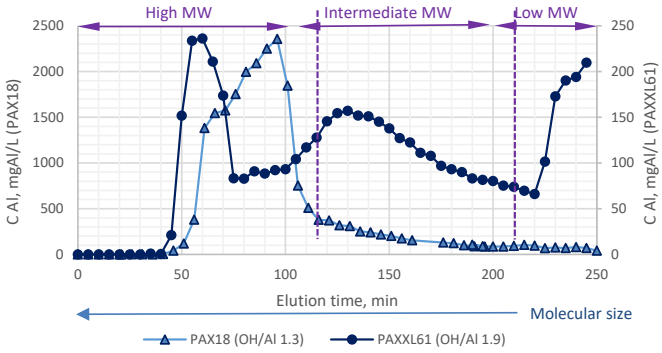

Figure 12. Size exclusion chromatograms of collected prepolymerized aluminium chloride (PACl) fractions.

According to the obtained chromatograms (Figure 12), the PAXXL61 sample was characterized by three different peaks, eluted by size exclusion mechanisms. The peaks were observed at elusion times 60 min, 130 min and 245 min, which refer to high, intermediate and low molecular weight bands, respectively. According to Brookes et al. [91] and Striegel [92], the retention time of the molecules in the chromatography column is inversely proportional to their molecular weights. Hence, the largest molecules are eluted at the lowest elution times, which is called an "inverse-sieving" mechanism. For PAXXL61, high MW fraction accounts for 39.1% of the total Al, intermediate MW

fraction exhibited 26.0% of the total Al and low MW isolate made up 34.9% of the total Al of the investigated prepolymerized aluminium coagulant with high basicity.

On the contrary, PAX18 was merely characterized by one broad peak eluted in 96 min. The obtained chromatography profile (Figure 12) suggests that high MW fraction accounts for about 85% of the total Al of the studied prepolymerized aluminium chloride with medium basicity.

High MW isolate of PAXXL61 was obtained 36 min earlier than for PAX18, pointing out that the tested prepolymerized aluminium chloride with high basicity and the incorporated SiO_2 had higher MW fractions in comparison to its counterpart with medium basicity. However, high MW isolates constitute less than half of the total Al in PAXXL61, which suggests they might not be the predominant contributor to the overall MW of the relevant compound.

3.5. Statistical Analysis

3.5.1. Partial Least Squares Regression Analysis

PLS regression analysis was performed for the ML samples from TRT with and without pH correction according to the following variables and response functions (Table 2).

Table 2. Model inputs.

Predictors (X)	Response (Y)
$MLSS_{in}$ [1], CST [2], turbidity, pH, D[4,3], D[3,2], span, uniformity, zeta potential, coagulant dosage (Dose)	Average normalized permeability ($_{av}P_N$), Filtration time (F)

Notes: [1] Initial mixed liquor suspended solids (MLSS of the raw sample); [2] Capillary suction time.

The obtained model was validated by applying random cross-validation in PLS. During the cross-validation, the dataset was divided into 20 segments. Some elements were taken out of analysis since they were indicated as potential outliers. The number of PLS components (factors), was chosen according to the explained variance.

Eventually, the following results were obtained (Figure 13).

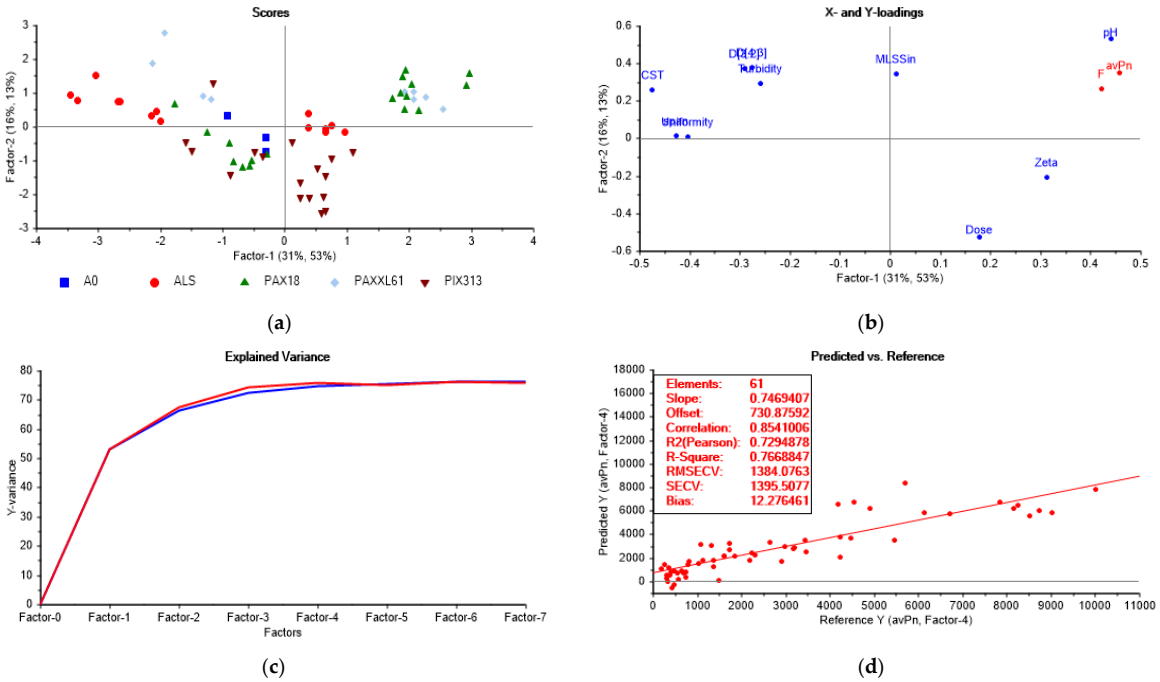

Figure 13. Results of partial least squares (PLS) of the data from the TRT-regression overview: (**a**) scores plot; (**b**) loadings plot; (**c**) total residual variance plot; (**d**) fouling intensity prediction model.

According to the acquired results (Figure 13), the first two factors describe 47.0% and 66.0% of the variance in the dataset for x and y, respectively.

The scores plot demonstrates the case with four distinctive clusters: the activated sludge samples treated with PAX18, PAXXL61, ALS and PIX313. Samples within a cluster contain similar samples. The difference between the clusters is explained by Factor-1 and Factor-2.

According to the PLS loadings plot, Factor-1 clearly describes span, uniformity, CST, zeta potential, pH, filtration time and the average normalized permeability. Factor-2 apparently accounts for D[4,3], D[3,2], turbidity, $MLSS_{in}$ and coagulant dose. From the loadings plot, all the variables appeared to be significant and provided stability and reliability to the model. Span and uniformity are highly positively correlated with each other and exhibit a positive link to CST, turbidity, D[4,3] and D[3,2]. Such PSD parameters as D[4,3] and D[3,2], have a positive correlation with each other. However, they show a negative correlation to coagulant dose and zeta potential. CST and turbidity are negatively linked to zeta potential and coagulation dose. Meanwhile, the coagulant dose is positively correlated with zeta potential. CST has a high negative correlation with the response variables and pH along Factor-1.

The total residual variance plot indicates how much of the variation in the data is described by the different numbers of factors [55,56]. According to the total residual variance plot (Figure 13), the highest explained Y-variance (76%) is attained while applying four factors and then reaches a plateau.

An analysis of the validation plot shows that the developed model is linear, has a R-squared value of 0.77 and has a good fit for the majority of data (i.e., slope = 0.75). The Root Mean Square Error of Cross Validation (RMSEV) and the standard error of cross-validation (SECV) are equal to 1384 and 1395, respectively. However, it is essential to acknowledge that the mentioned errors have the same units as the reference Y (in this case, the average normalized permeability, $_{av}P_N$). R-squared (Pearson) is close to R-squared correlation (0.73 vs. 0.85), which indicates the reliability of the model. The developed model has a relatively low bias equal to 12.3, indicating that it has a low tendency to over- or underestimate the validation values. Hence, the developed model demonstrates a good prediction capability, which proves its reliability and high potential to be used during further stages when the operating conditions applied in this work are replicated.

In order to determine a predominant mechanism, which governs the behaviour of every coagulant, the data-driven sample grouping was automatically performed by equally dividing the band of the target parameter values in the whole range between the upper and lower limits into five groups. As a result, the relevant ranges were generated (Figure 14).

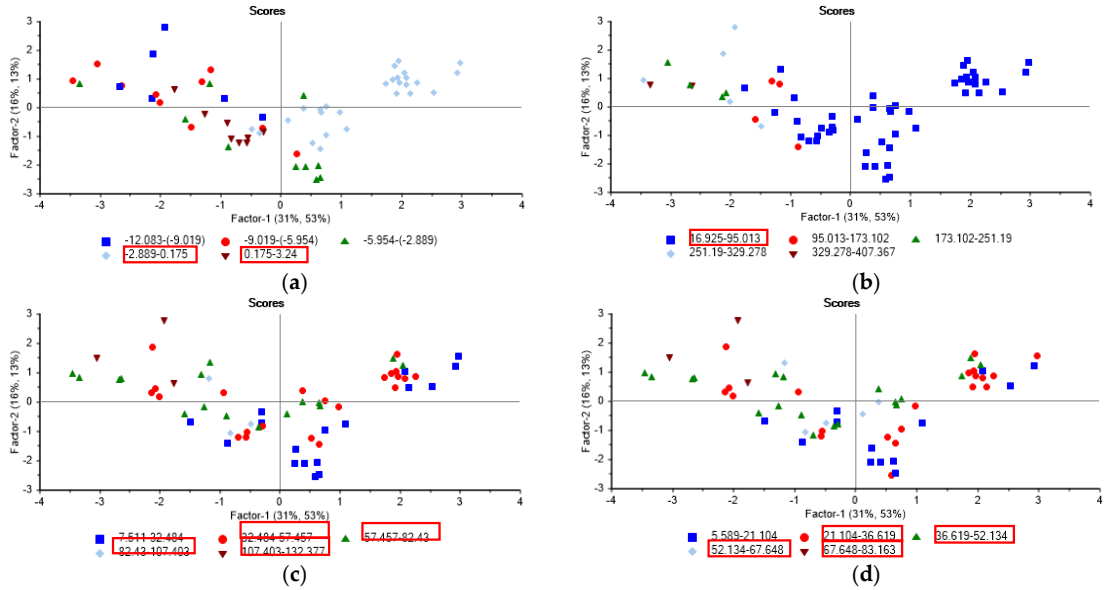

Figure 14. Results of partial least squares analysis (PLS) for the tested membrane flux enhancers—scores plot with the sample grouping according to: (**a**) zeta potential; (**b**) CST; (**c**) D[4,3]; (**d**) D[3,2].

The target levels of interest (marked with the red rectangles in the legends in Figure 14) were chosen in accordance with the variables: for zeta potential, the upper limit of values (group −2.9–3.2 mV); for CST, the lower boundary (group 17.0–95.0 s); and for the volume/mass moment mean, the range of higher values, including the upper boundary (group 32.5–132.0 µm/21.0–83.0 µm). This selection was congruent with the main mechanisms of fouling control: adsorption/charge neutralization (preferential decrease of zeta potential absolute value), the increase of relative hydrophobicity of the flocs (the decrease of dewaterability) and the increase of the mean particle size. According to the obtained PLS scores plot (Figure 14), the ranking trend among the studied coagulants, in decreasing order of dominance of each particular fouling mitigation mechanism, can be classified as:

- enhanced adsorption/charge neutralization (zeta potential −2.9–3.2 mV): PAX18 (100% of all PAX18 samples) > PAXXL61 (55.6%) > PIX313 (41.0%) > ALS (36.0%);
- the increase of relative hydrophobicity of the flocs (CST 17–95 s): PAX18 (100%) > PIX313 (82.0 %) > PAXXL61 (56.0%) > ALS (43.0%);
- the increase in particle size (D[4,3] 32.5–132 µm/D[3,2] 21–83 µm): ALS (100/100%) > PAX18 (78.0/94.0%) > PAXXL61 (78.0/78.0%) > PIX313 (41.0%/53.0%).

It was decided to denominate the mechanism of fouling inhibition as dominant if 55.0% or more of a total number of the samples of every coagulant is characterized by the above-mentioned ranges of the monitored parameters. As determined earlier (during the analysis of the TRT with pH correction), based on Figure 7e, the highest level of COD_{dis} removal (i.e., the reduction of the SMPs content) was observed for the majority of samples of prepolymerized aluminium coagulants PAXXL61 and PAX18 (100% and 67.0%) and iron (III) sulphate PIX313 (67.0%) for a total number of the samples in the selected dosage range, respectively. Consequently, the principal mechanism differs depending on the coagulant nature (Table 3).

Table 3. Prevailing mechanisms of action for the tested coagulants.

Mechanism of Action Coagulant	Enhanced Adsorption/Charge Neutralization	The Increase in Relative Hydrophobicity of the Flocs	The Increase in Particle Size	The Reduction of the SMPs Level
PAX18 (OH/Al 1.3)	+	+	+	+
PAXXL61 (OH/Al 1.9)	+	+	+	+
PIX313 (OH/Fe 0)		+		+
ALS (OH/Al 0)			+	

3.5.2. Two-Level Factorial Design of the Experiment

A factorial design was built in order to characterize how the selected factors interact and individually affect the fouling mitigation process and to determine the optimum combination of factor levels, that simultaneously satisfy the criteria of the maximum permeability/filtration time for the chosen coagulant.

The Average Permeability

To study the possible options of permeability maximization systematically, a two-level alternative factorial design was set up on the key factors: pH, temperature, MLSS and coagulant dose with two replicates (Tables 4 and 5).

Table 4. Factors and levels for two-level alternative factorial design.

Factor	Units	Low Level	High Level
pH	-	5.5	6.5
Temperature	°C	20	25
MLSS	g/L	4.0	6.0
D [1]	µmoleAl/mgSS	1.1	1.9

Notes: [1] Coagulant dose.

Table 5. Layout for a designed experiment.

	Factor 1	Factor 2	Factor 3	Factor 4	Response 1
Run	A:pH	B:Temperature, C	C:MLSS, g/L	D:D, µmolAl/mgSS	Permeability, LMH/bar
1	5.5	20	4.0	1.1	8725.6
2	6.5	25	6.0	1.9	6614.1
3	6.5	20	6.0	1.1	2055.5
4	5.5	20	4.0	1.1	8698.6
5	5.5	25	4.0	1.9	12,204.9
6	5.5	25	6.0	1.1	7146.1
7	6.5	20	4.0	1.9	10,020.4
8	6.5	25	6.0	1.9	6578.7
9	6.5	20	4.0	1.9	10,046.9
10	6.5	25	4.0	1.1	11,168.8
11	6.5	20	6.0	1.1	2024.6
12	6.5	25	4.0	1.1	11,196.9
13	5.5	20	6.0	1.9	6827.6
14	5.5	25	6.0	1.1	7169.4
15	5.5	20	6.0	1.9	6859.4
16	5.5	25	4.0	1.9	12,233.0

A preliminary analysis was conducted to understand the general relationships between the factors and the response function before carrying out an in-depth analysis. The relevant graphs (Figure S1) represent the impact of every factor on the permeability.

According to the obtained plots (Figure S1), coagulant dose and temperature are positively linked to the average permeability, while the increase in pH and MLSS cause the permeability to drop.

This analysis was followed by the use of more sophisticated tools.

The values of the response function ranged from 2024.6 to 12,233.0, which results in a ratio of its maximum to a minimum value of 6.04, which is greater than 3, indicating a high potential for the model improvement [93,94]. In the current work, a power family of transformations $y^* = y^\lambda$ (λ, the transformation parameter; y, the observed response function; y^*, the transformed response function) was selected. The transformation of the response function was performed in order to increase the fit of the model to the data. An empirical graphical technique in the form of a Box-Cox plot (the graph is not presented) was applied to determine the optimum transformation parameter λ of the response function. As the present study discovered, the value of λ equal to 1.61 resulted in the minimum residual sum of squares. Therefore, power transformation was chosen at the beginning of the analysis, applying $\lambda = 1.61$.

In order to detect the important effects among the variables and their interactions, the analyses of a half-normal plot and Pareto chart (Figure 15) were carried out.

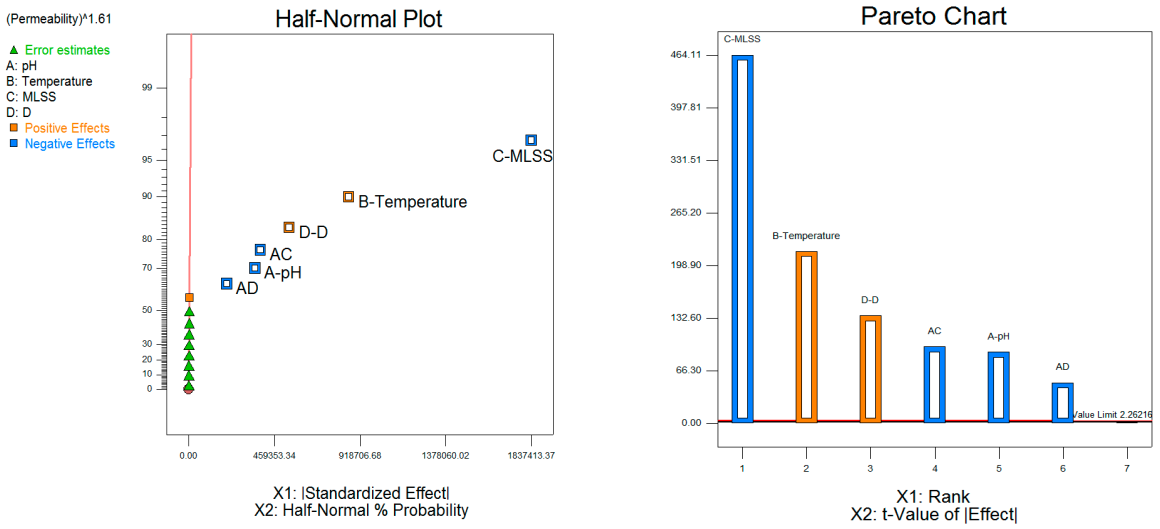

Figure 15. The selection of the effects to be modelled: (**a**) half-normal plot of effects; (**b**) Pareto chart.

The half-normal plot of effects demonstrates the absolute values of the squares of effects plotted against their cumulative normal probabilities [93,94]. The terms, which were selected as significant, that is, included in the model, were C (MLSS), B (temperature), D (coagulant dose), AC (the interaction effect of pH·MLSS), A (pH) and AD (the interaction effect of pH·coagulant dose). The negligible effects lined up at the red "error line" close to zero (Figure 15a).

The Pareto chart (Figure 15b) indicates the magnitude of the selected effects. The plot shows that all the selected effects are higher than Bonferroni limit = 3.46159 and t-value limit = 2.26216 (t value can be identified as a magnitude of the difference relative to the variations in the data [95]).

Analysis of variance (ANOVA) (Table 6) provides a set of formulas that enable the computation of test statistics and confidence intervals [96]. It gives the necessary evidence of the overall model significance, the importance of each coefficient, model accuracy and reliability, the possibility of model improvement and model application to navigate the design space.

Table 6. Analysis of variance table for the selected factorial model (Partial sum of squares-Type III).

Source	Sum of Squares	Df [1]	Mean Square	F-Value	*p*-Value Prob > F	
Model	1.89×10^{13}	6	3.15×10^{12}	50178.2	<0.0001	significant
A-pH	5.06×10^{11}	1	5.06×10^{11}	8074.3	<0.0001	
B-Temperature	2.95×10^{12}	1	2.95×10^{12}	47019.0	<0.0001	
C-MLSS	1.35×10^{13}	1	1.35×10^{13}	2.154×10^{5}	<0.0001	
D-D	1.16×10^{12}	1	1.16×10^{12}	18486.6	<0.0001	
AC	5.92×10^{11}	1	5.92×10^{11}	9434.2	<0.0001	
AD	1.67×10^{11}	1	1.67×10^{11}	2659.4	<0.0001	
Residual	5.64×10^{8}	9	6.27×10^{7}			
Lack of Fit	6.05×10^{7}	1	6.05×10^{7}	0.96	0.3557	not significant
Pure Error	5.04×10^{8}	8	6.3×10^{7}			
Corrected Total	1.89×10^{13}	15				

Notes: [1] the numerator degrees of freedom.

Fisher's value (F-value) is the ratio of the "between-group variance" (the variation as a result of the intentional experimental manipulation) to the uncontrollable "within-group or error variance" [97]. The model's F-value is equal to 50,178.2, which indicates the significance of the derived model. There is only a 0.01% chance that an F-value this large could occur due to noise.

Besides, based on the *p*-values (<0.05), it can be concluded that the derived model was significant and all the selected factors, such as pH, temperature, MLSS, coagulant dose and the interaction terms pH·MLSS and pH·coagulant dose had a significant effect on the model. Otherwise, the *p*-values greater than 0.1 would have indicated the insignificance of the model terms.

The model was characterized by R-Squared equal to 1, which indicates its linearity.

The predicted R-Squared of 0.9999 was in reasonable agreement with the adjusted R-Squared of 1, that is, the difference was less than 0.2. "Adequate Precision," which measures the signal to noise ratio, was equal to 685.5, which is the evidence of an adequate signal. Therefore, this model can be used to navigate the design space. The "Bayes information criterion" (BIC) and the "Akaike information criterion" (AIC) determine which model from the set of models describes the dataset in the best way. The criteria take into consideration model complexity and serve as barriers to model overfitting. The distinctive feature of BIC is its consistency, which helps to select a lower dimensional model when it is the most accurate. The model, which has the highest BIC or AIC criterion, fits data best, therefore, should be selected [98,99]. In the current model, BIC and AIC criteria were equal to 342.9 and 351.5, respectively, which indicates a consistent fit of the model with the response data.

After determination of the model coefficients the final equations can be derived (Equation (5) and (6)).

Final equation in terms of coded factors:

$$(\text{Permeability})^{1.61} = 2.100 \times 10^6 - 1.779 \times 10^5 \cdot \text{A} + 4.292 \times 10^5 \cdot \text{B} - 9.187 \times 10^5 \cdot \text{C} + 2.691 \times 10^5 \cdot \text{D} - 1.923 \times 10^5 \cdot \text{AC} - 1.021 \times 10^5 \cdot \text{AD}, \quad (5)$$

where A is a coded value for pH, B is a coded value for temperature, C is a coded value for MLSS, D is a coded value for the coagulant dose, AC is a coded value for pH·MLSS and AD is a coded value for pH·coagulant dose.

It is worth noting that the equation with respect to coded or actual factors can be used to make predictions about the response for given levels of each factor. In the case of coded factors, the high levels of the factors correspond to +1 and the low levels of the factors are coded as −1. According to the derived equation, MLSS, temperature and the coagulant dose have the highest impact on the average permeability.

Final equation in terms of actual factors, which can be applied to make the predictions about the average permeability for the specified factorial levels:

$$(\text{Permeability})^{1.61} = -1.21741 \times 10^7 + 2.33256 \times 10^6 \cdot \text{pH} + 1.71694 \times 10^5 \cdot \text{Temperature} + 1.38853 \times 10^6 \cdot \text{MLSS} + 3.73531 \times 10^6 \cdot \text{D} - 3.84539 \times 10^5 \cdot \text{pH} \cdot \text{MLSS} - 5.10408 \times 10^5 \cdot \text{pH} \cdot \text{D}, \quad (6)$$

where D is a coagulant dose.

The last equation implies that the levels should be specified in the original units for each factor. This equation is not applicable for the determination of the relative impact of each factor since the coefficients are scaled to correspond to the units of each factor and the intercept is not at the centre of the design space [94].

Regression diagnostics provide the validation analysis of the derived model. In the current work, it includes a normal probability plot, which describes the distribution of model errors; a plot of the residuals against the fitted values to assess the independence of the error terms and system stability; and Cook's distance plot for the identification of the outliers (Figure 16).

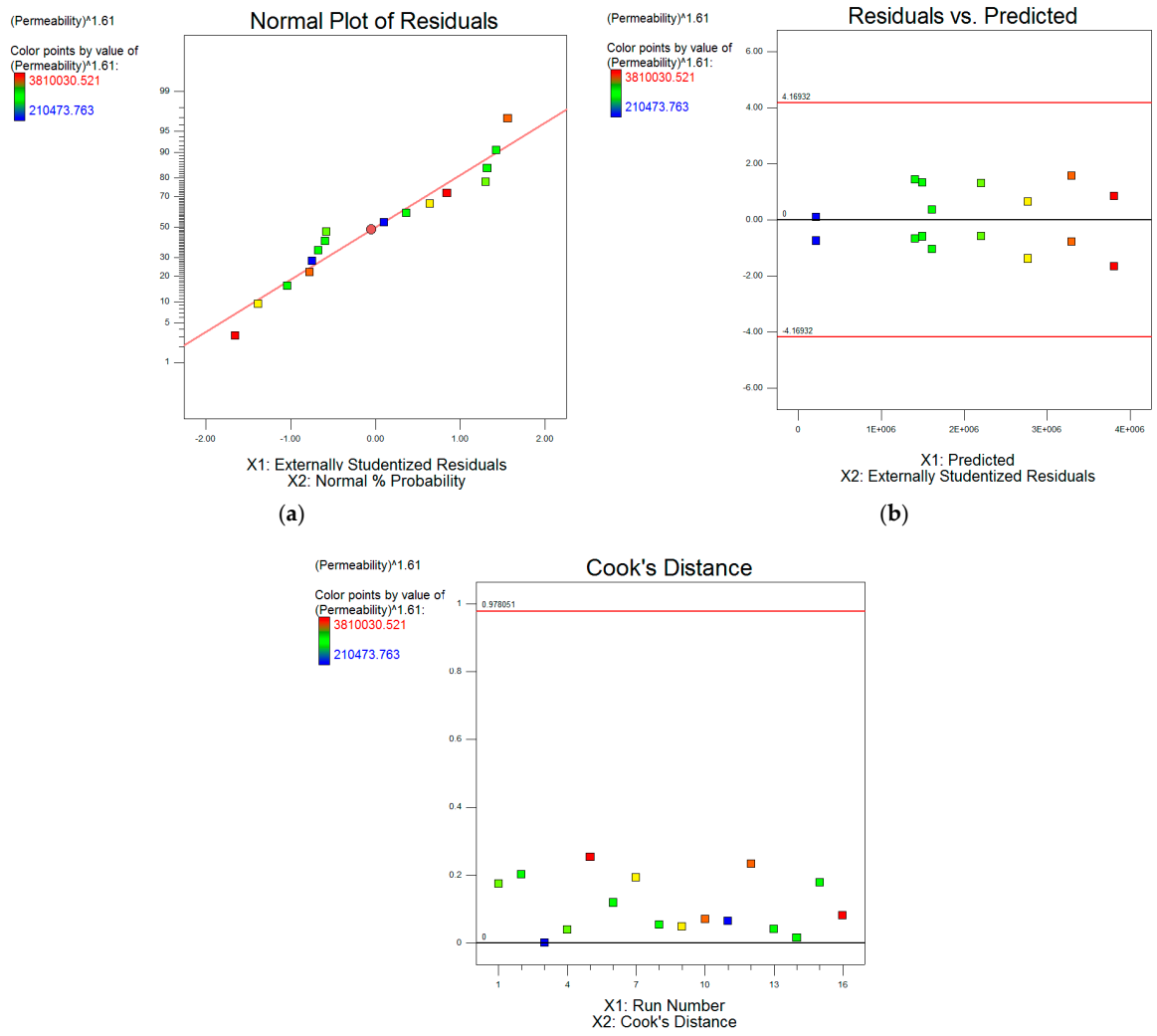

Figure 16. Model diagnostics plots: (**a**) normal probability plot; (**b**) residuals versus predicted response; (**c**) Cook's distance vs. the run.

The normal probability plot demonstrates the residuals plotted against the normal scores (expected residuals values) under the assumption of normality [96]. According to the obtained results (Figure 16a), there is a clear linear trend between the residual values and normal scores in this model, indicating that the errors are normally distributed, thus the normality assumption is satisfied.

Residuals versus predicted response values plot (Figure 16b) demonstrates that all the residuals exhibit a fairly uniform spread along Y-axis, that is, no steady upward/downward trends are observed, starting from the first residual and ending with the last one. Hence, the size of the residual is independent of the predicted response value.

Cook's distance quantifies the regression change, if needed, to exclude any of the samples from the analysis. It is an overall measure of the distances between the pairs of the regression coefficients: $\hat{\beta}_0$ and $\hat{\beta}_0{}^i$, $\hat{\beta}_1$ and $\hat{\beta}_1{}^i$ and so on. $\hat{\beta}^i$ coefficient stands for the estimate of the $\hat{\beta}$ coefficient when the ith sample is removed from the analysis. The calculation of the Cook's distance is carried out according to the following equation [96]:

$$D_i = \frac{(y_i - \hat{y}_i)^2}{(k+1)\cdot \mathrm{MSE}} \cdot \left[\frac{h_i}{(1-h_i)^2} \right], \quad (7)$$

where h_i. is leverage; k is the number of β-coefficients in the model, including the intercept; $y_i - \hat{y}_i$ (a deleted residual) is a difference between the actual response and the predicted response value which is obtained when the ith sample is excluded from the analysis; MSE is the mean squared error for the fitted model [94,96].

According to the obtained graph (Figure 16c), there is no sample that shows a high value of Cook's distance: all the samples have Cook's distance substantially lower than 1. Therefore, one can conclude that all observed responses have a weak impact on the estimates of the regression coefficients, that is, neither large leverages nor large residuals can be identified, which is the evidence of the absence of the outliers in the current model.

The interpretation of the selected model can be made by analysing model graphs (Figure 17).

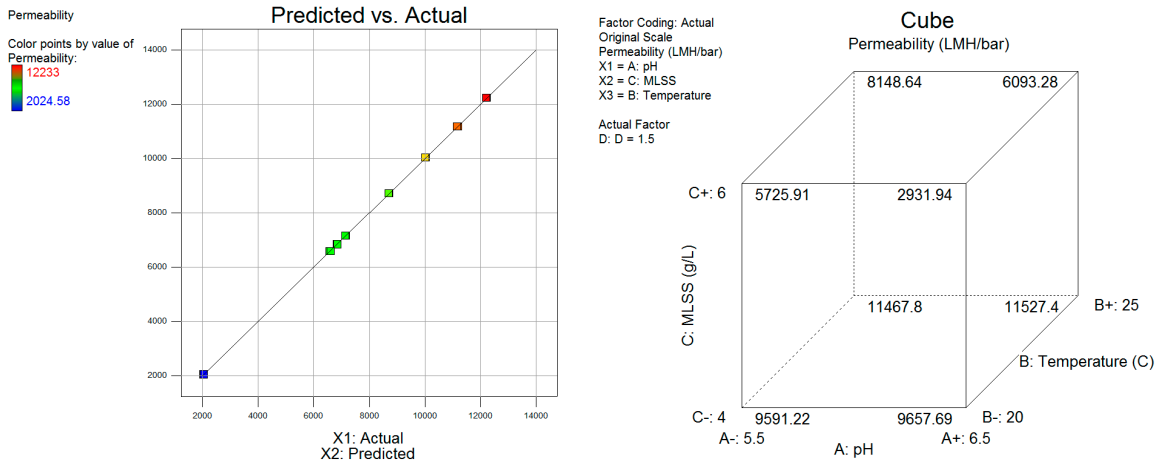

Figure 17. Model graphs of the factorial design: (**a**) predicted vs. reference plot; (**b**) cube plot, k = 3, D = 1.5 μmole Al/mgSS.

According to the predicted versus reference plot (Figure 17a), the predicted values fully correspond to the actual values, which indicates a high accuracy of the derived model.

The cube plot (Figure 17b), demonstrates the average predicted values of the response function superimposed on the eight corners, of the cube, at the combinations of high and low levels of the three factors, that have significant effects: MLSS, pH and temperature at the selected actual value of the coagulant dose (1.5 μmole Al/mgSS in the represented plot) [94,100]. According to the represented graph, the highest levels of the average permeability 11467.8–11,527.4 LMH/bar can be attained at minimum MLSS (4 g/L) and maximum temperature (25 °C) (values calculated at D = 1.5 μmole Al/mgSS). Meanwhile, pH has a minor positive effect at the low level of MLSS and an adverse effect at a high MLSS level.

The optimization analysis determines the settings or values of the significant factors, which provide the desired values of the response function, based on the placed criteria [100].

In the current work, the optimization is based on the maximization of the desirability function (D), which is a converted response function. In this case, the overall desirability is equal to the individual desirability function d since there is just a single response function. In the case of response maximization, D would equal 1, if the response function is at its target value; D would equal 0 if the value of the response function is undesirable [93,100].

The determination of the important factorial levels, which provided the maximum permeability yield was conducted. Two cases were tested, which differed from each other in the requirements, imposed on the values of the factors. In the first case, the goal was to maximize the response function, while varying pH, MLSS, temperature and coagulant dose in the relevant ranges, defined by high and low factorial levels, provided in Table 4. As a result, according to one of 94 possible solutions for

optimization, the maximum average permeability, equal to 12,222.8 LMH/bar, was attained at pH 5.5, temperature 25 °C, MLSS 4 g/L and coagulant dose 1.9 μmolAl/mgSS (Desirability = 0.999).

In the second case, the purpose remained the same—to maximize the average permeability. However, under harsher conditions, these parameters were imposed on the factors: temperature and coagulant dose were kept at a low level, around 20 °C and 1.1 μmolAl/mgSS, respectively, while MLSS was constrained to its maximum tested level of 6 g/L. Consequently, according to one of the 94 possible solutions for optimization, the highest average permeability was equal to 4750.9 LMH/bar at pH 5.5 (Desirability = 0.707).

Point prediction and confirmation were used to compute a single value for the response function and interval estimates, using the developed regression model. The estimation procedure establishes the weights of the regression model to minimize the difference between the predicted and actual values of the response function. Consequently, the predicted value represents the total of all effects of the regression model and turns the residuals into a validation measure for the overall model performance [101]. Confirmation is the second stage of post-analysis; of which the purpose is to confirm that the model can predict the actual dependent variable at the optimum settings of parameters determined during the optimization. The results of point prediction and confirmation are represented in Table S6.

The results of the point prediction and confirmation for the average permeability ($_{av}$P) function indicated that at pH 5.5, temperature 25 °C, MLSS 4 g/L and Dose 1.9 μmolAl/mgSS the predicted mean permeability is 12,222.8 LMH/bar with the standard deviation between the predicted and actual $_{av}$P value equal to 15.8 LMH/bar at a 95% confidence interval. Meanwhile, (at pH 5.5; temperature 20°C; MLSS 5.92 g/L; and dose 1.1 μmole Al/mgSS) the predicted mean permeability is equal to 4750.9 LMH/bar with the standard deviation between the predicted and actual $_{av}$P value equal to 28.1 LMH/bar at a 95% confidence interval.

The obtained values of standard deviation are the indication of high accuracy of the developed regression model.

Consequently, the developed model can be used to determine the optimum conditions of the PAX18 application, which would provide the highest yield of the average permeability in accordance with the desired factor settings.

Filtration Time

The same sequence of analysis procedures was applied to the experimental design with the filtration time as a response function for the levels of factors, defined in Table 4. During the experiment, filtration time values were in the range 5–120 min, depending on the levels of the parameters, therefore it was decided to select power family of transformations as in the case of the average permeability in order to increase the fit of the model to the data. According to the relevant Box-Cox plot (not shown), the optimum transformation parameter λ of the response function, which resulted in the minimum residual sum of squares, was equal to 3. Therefore, power transformation was chosen at the beginning of the analysis, applying λ = 3.

According to ANOVA, the overall model and every selected factor were found to be significant, having the *p*-values < 0.0001. The model F-value was equal to 6.36×10^6, indicating model significance. R-squared values > 0.9999 demonstrated model linearity and the signal to noise ratio, equal to 4627, provided evidence of an adequate signal. Consequently, this model can be used to navigate the design space.

As a result, the final equation in terms of coded factors for the filtration time was as follows:

$$\begin{aligned}(\text{Filtration time})^3 = 8.68 \times 10^5 - 3165.47 \cdot A - 1144.71 \cdot B + 3165.47 \cdot C + 1144.71 \cdot D \\ + 8.598 \times 10^5 \cdot AC,\end{aligned} \quad (8)$$

where A is a coded value for pH, B is a coded value for Temperature, C is a coded value for MLSS, D is a coded value for the coagulant dose, AC is a coded value for pH·MLSS.

Equation (8) demonstrates that the interaction factor pH·MLSS has the highest influence on the filtration time. The other factors have relatively identical impacts on the response function.

Final equation with respect to actual factors:

$$(\text{Filtration time})^3 = 5.25 \times 10^7 - 8.6 \times 10^6 \cdot \text{pH} - 457.9 \cdot \text{Temperature} - 1.03 \times 10^7 \cdot \text{MLSS} + 2861.8 \cdot \text{D} + 1.72 \times 10^6 \cdot \text{pH} \cdot \text{MLSS} \quad (9)$$

According to Equation (9), temperature and coagulant dose have the lowest coefficients; however, these results cannot serve as a basis for making the conclusion about the magnitudes of the model coefficients. Equation (9) is applicable merely to making the predictions about the filtration time using the provided levels of factors.

The results of diagnostics demonstrated the fulfilment of the normality assumption in the current model and the absence of the outliers.

The interpretation of the factor interactions in the derived model was provided by analysing the cube plot (Figure 18).

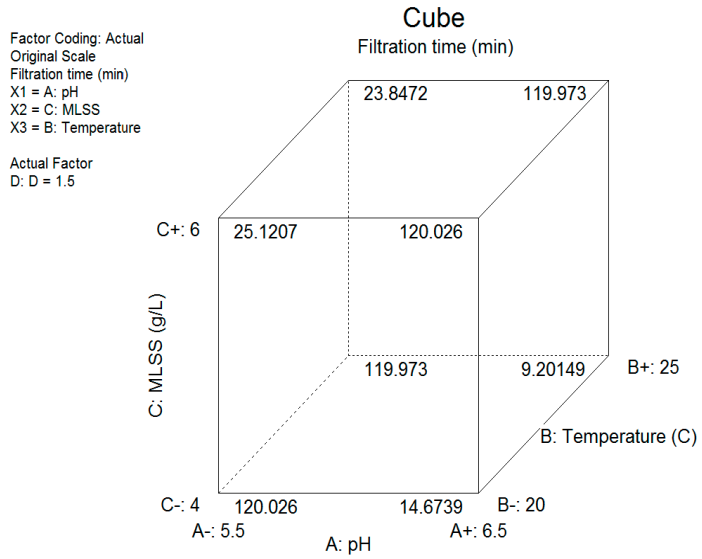

Figure 18. Cube plot of the factorial design (k = 3, D = 1.5 µmole Al/mgSS).

The cube plot (Figure 18) demonstrates the changes in the filtration time depending on pH, MLSS and temperature at constant coagulant dose. The obtained results show an ambiguous effect of pH on the response function, which highly depends on the MLSS. At the low MLSS level 4 g/L the increase of pH from 5.5 to 6.5 drastically reduces the filtration time from 120 to 9–15 min, whereas at the high MLSS level—6 g/L, the pH increase exhibits the opposite effect: the increase of filtration time from 23.8–25.1 to 120 min. In addition, a minor negative impact of temperature on the filtration time can be observed.

According to the represented cube plot, the filtration time is maximum (120 min) at:

(1) A+1 (pH 6.5), B-1 – +1 (T = 20–25 °C), C+1 (MLSS 6 g/L) (values calculated at D = 1.5 µmole Al/mgSS);
(2) A−1 (pH 5.5), B-1 – +1 (T = 20–25 °C), C−1 (MLSS 4 g/L) (values calculated at D = 1.5 µmole Al/mgSS).

The results of the numeric optimization indicated that for the provided upper and lower levels of factors with no specific requirements, imposed on the factors values, the maximum filtration time yield

equal to 120 min could be attained applying pH 6.5, temperature 20.7, MLSS 5.9, coagulant dose 1.69 (Desirability = 1). If temperature and coagulant dosage are minimized (20 °C and 1.1 µmole Al/mgSS), while MLSS is maximized 6 g/L, the maximum filtration time equal to 120 min is attained at pH 6.5 (Desirability = 1). The provided solutions represent one out of 94 possible solutions for optimization in each case of the parameter settings.

The results of the post-analysis (point prediction and confirmation) for the filtration time function indicated that at pH 6.5, temperature 20.7 °C, MLSS 5.9 g/L and Dose 1.69 µmol Al/mgSS the predicted mean filtration time is 118 min with the standard deviation 0.0146 at a 95% confidence interval. Meanwhile, (at pH 6.5; temperature 20 °C; MLSS 6 g/L; and dose 1.1 µmole Al/mgSS) the predicted mean filtration time is equal to 120 min with the standard deviation 0.0141 at a 95% confidence interval.

Hence, the developed model can be used to determine the optimum conditions of the PAX18 application, which provide the highest yield of the filtration time in accordance with the desired factor settings.

4. Discussion

The acquired results demonstrated the importance of the electrokinetic potential, relative hydrophobicity of the flocs expressed through capillary suction time (CST), the mean particle size/particle size distribution, chemical oxygen demand (COD) and mixed liquor suspended solids (MLSS) for the characterization of the biomass fouling propensity.

The influence of MLSS, COD and relative hydrophobicity (RH) on the fouling potential of mixed liquor in the pilot scale BF-MBR agrees with the findings of our previous work [42]. According to both studies, the increase in MLSS mainly exhibited a negative influence on the average permeability. This effect could be explained by the fact that elevated MLSS content tends to induce severe reversible fouling, high ML viscosity and the production of biopolymers [102–104]. The current research together with the study by Kulesha et al. [42] also revealed that the reduction of COD positively contributes to fouling mitigation. The findings corresponded to the conclusions of different research groups [15,105–108], who identified a positive link between COD levels and irreversible fouling in MBR, which was induced by the increased production/release of soluble microbial products (SMPs). RH of the floccules was found to have a minor positive link to permeability slope [42]. However, the present study pointed out a significance of the RH for characterization of the biomass fouling propensity and its positive correlation with the permeability. These findings agree with different research works [109–111], where the increased RH had a positive contribution to membrane fouling mitigation, improved flocculation and dewaterability of activated sludge in the MBR systems. A greater fouling potential of the hydrophilic organic fractions was admitted by Johir et al. [112], Qin et al. [113], Shen et al. [114] and Pramanik et al. [115]. Mu et al. [116] used multivariate statistics to study the relationships between RH, the other physicochemical properties of the mixed liquor constituents and the fouling rate in MBR with PVDF modules. The analysed substances were classified as hydrophobic/hydrophilic based on the critical retention factor. Statistical analysis revealed a close relation of RH to the aromaticity of the organic matter and a strong correlation between the molecular weight (MW) > 10 kDa of the foulants and the fouling rate. As found out, nominally strong hydrophilic or strong hydrophobic fractions do not contribute to the membrane fouling but rather "moderately" hydrophobic/hydrophilic substances with high MW.

The CST parameter indicates the dewaterability of the sludge floccules [24,117] and has been used as a fouling indicator in MBR systems [118,119]. CST is positively linked to the concentration of biopolymers in ML and has a negative correlation with the permeability [120–122].

According to the recent findings, CST has an additional valuable property with regard to the characterization of the biomass fouling propensity, which is its relation to relative hydrophobicity of the flocs. The negative correlation between these two parameters was confirmed by the analysis of the data acquired from the previously investigated pilot plant [42] (the loadings shown in Figure S2),

where relative hydrophobicity was in the range 30.0–67.5%, while CST values were in the range 65.6 –141.2 s.

According to the loadings plot (Figure S2), CST is highly negatively correlated to relative hydrophobicity. This observation can be explained by the fact that if relative hydrophobicity of the flocs is high, its free water is less firmly attached to the microstructure of the microbial flocs due to the low affinity of water for their hydrophobic surface. Consequently, less time is required for water to be released on the filter paper and to reach the outer circle during the CST measurement.

A significant impact of relative hydrophobicity on the dewaterability of the microbial flocs was also reported by Jin et al. [123]. However, their findings showed the opposite tendencies, which was, probably, due to low CST values and their low variance in the experiment (~12.5–17.5 s).

Time-to-Filter (TTF) is a parameter of ML filterability, which is correlated with CST and is occasionally used in the MBR investigation practice [117,124,125]. In a study by Gkotsis et al. [40], TTF was used as the indicator of reversible fouling and as a variable for the determination of filterability enhancement during the batch filtration tests. On the contrary, as admitted by Fan et al. [126], the static conditions, which were applied during the TTF method, involved different mechanisms of particle agglomeration on the membrane surface, than those, during the MBR filtration cycle, thus making this parameter a poor indicator of the critical flux in MBR.

In the current research, the elevated TTF levels in the overdosing regions for TRT applying the pH adjustment appeared to be a good indicator of the deterioration of the mixed liquor filterability. However, we incline to the idea that TTF is an auxiliary parameter for the characterization of biomass fouling potential, which, if necessary, can be determined based on its correlation with CST.

According to different studies [61,127,128], the surfaces of EPSs and SMPs contain ionogenic functional groups such as –OH; –COOH; $–OPO_3H_2$, $–OSO_3$, $–OC_3H_5O_3$ (glycerate), $–OC_3H_3O_2$ (pyruvate) and $C_4H_4O_4$ (succinate), which have a high affinity towards polyvalent metal ions and, at neutral and slightly alkaline pH, bear negative charges.

The decrease of the absolute value of electrokinetic potential (ζ-potential) of mixed liquor was among the central tasks of the experiments, conducted in the present study. Electrokinetic potential is a key parameter for characterization of the interaction between the ML foulants and the membrane surface, assessment of the biomass fouling propensity and efficiency of chemical flux enhancement via the charge neutralization mechanism in MBR/BF-MBR systems [15,110,129–132].

The present study assessed the flocculating ability of the flux enhancements based on the parameters of the particle size distribution. Particle size distribution/mean particle size is another important characteristic of mixed liquor in MBR/BF-MBR, which was investigated by different research teams [23,131–135]. The increase in mean particle size can play a crucial role in terms of fouling mitigation due to the potential shift of the fouling type from irrecoverable or irreversible to reversible, drastically improving the efficiency of membrane cleaning and fouling mitigation. Besides, the increase in size of the particles facilitates their back transport (shear-induced diffusion) from the membrane surface to the bulk solution and surface erosion (scouring of the membrane surface by flocs), which positively contribute to the flux enhancement [9,33,136]. The decrease in particle size over time indicates the deflocculation of the formed aggregates due to their inability to resist the shear forces [137]. Floc breakage can result in the release of SMPs to mixed liquor and, consequently, more severe membrane fouling.

Partial least squares analysis (PLS) and principal component analysis (PCA) were applied in different studies on membrane fouling in MBR [57,138–142]. Even though various fields of chemistry and industrial process control can benefit from the use of these multivariate chemometric analysis [143], its application for the analysis of the fouling development and mitigation in membrane systems, particularly in BF-MBR, is still quite limited. In the work by Kulesha et al. [42], PLS-regression analysis was used for developing the fouling prediction and control strategy based on the interrelation between the mixed liquor characteristics, fouling indicators and the operating conditions. Average normalized permeability and its slope were found to be the most reliable fouling indicators. The present study,

as well as our previous work [42], proved that multivariate chemometric approach based on (PLS), that is, PLS-regression (PLSR), is a reliable tool for characterization, prediction and control of membrane fouling in the BF-MBR.

Systematic research, demonstrated in the current work, develops the concept of chemical flux enhancement in the biofilm membrane bioreactor (BF-MBR) based on an adsorption/charge neutralization mechanism, revealed from the comparative study of prepolymerized and non-prepolymerized inorganic coagulants through the chemometric approach to membrane fouling control and optimization of membrane filtration.

The underlying hypothesis was that prepolymerized aluminium chloride (PACl) coagulants have a higher potential to improve the filtration performance of the BF-MBR system in wastewater treatment applications than the non-prepolymerized ones [35]. Neither of the currently found studies on chemical flux enhancement in BF-MBR could prove this hypothesis [22,35], despite the fact, that prepolymerized aluminium coagulants were reported to be more efficient than their non-prepolymerized counterparts in coagulation/flocculation processes with regard to removal of particulate and colloidal matter [36,144], likewise in membrane flux enhancement in MBRs [38,39].

The current research demonstrated that the general mechanisms of fouling mitigation in BF-MBR, are almost the same as in MBR systems, defined in our previous study [7], thus the observations on MBR systems could be continued for BF-MBR systems and the mechanisms of processes were studied and explained in this work.

Apart from defining the mechanisms of coagulant action, our previous work [7], reported that different bacterial solid surfaces have readily ionizable functional groups, which are pH dependent, and, a negative surface charge prevails merely at alkaline pH. The latter part of the statement was not confirmed in the current work during the analysis of the raw mixed liquor, where the zeta-potential values of the samples with no coagulant addition or pH adjustment were negative −14.01–(−11.5) mV at acidic/neutral pH_{raw} 5.1–7.0 and temperature 17.1–23.1 °C. The negative charge of the mixed liquor system at neutral pH corresponds to the previous findings [128], while the presence of the negative biomass charge under acidic conditions still remains unclear. The potential reasons could be: (1) a complex composition of the mixed liquor, which consists not merely of the bacteria but also of the viruses, fungi, single-celled organisms, dead cells and products of their decay; (2) the release of organically bond nitrogen from the biodegradable organics and its subsequent nitrification in the MBBR part, entailing its oxidation to nitrites (NO_2^-), which are further oxidized to nitrates (NO_3^-), influencing the charge of the system.

The current research defined the necessity of the pH adjustment before and during the coagulant addition to provide complete coagulation of the mixed liquor according to Le Chatelier's principle. The efficiency of the studied coagulants was highly improved by pH adjustment, conducting coagulation at optimum pH levels: 5.5–6.0 for prepolymerized aluminium chloride coagulants, 4.5 for aluminium sulphate and 3.8–4.1 for iron (III) sulphate.

The observations of the superior performance of prepolymerized coagulants regarding fouling mitigation in the current research agree with the studies by Wu et al. [38] and Chen and Liu [39]. However, Ivanovic and Leiknes [22,35] made the conclusions, which contradict to Wu et al. [38] and Chen and Liu [39], as well as with the results of our work.

The concept, presented in the current work, is advantageous, since it serves as a bridge between the flux enhancement mechanisms, mixed liquor fouling propensity, filtration parameters and characteristics of the tested coagulants, employing the statistical approaches, which helps to create a more comprehensive picture of fouling mitigation and prediction to solve the existing dilemma.

According to the obtained results, the extent of chemical flux enhancement in the BF-MBR system highly correlated with the resulting system charge, being strongly affected by the intrinsic charge concentration of the coagulants and their basicity. The ranking trend among the studied coagulants in decreasing order of fouling mitigation can be classified as: PACl with medium basicity (OH/Al 1.3, 0.97 μequiv./mg_{salt}) > PACl with high basicity (OH/Al 1.9, 0.65 μequiv./mg_{salt}) > $Fe_2(SO_4)_3$

(OH/Fe 0, 0.26 μequiv./mg_{salt}) ≈ $Al_2(SO_4)_3$ (OH/Al 0, 0.06 μequiv./mg_{salt}). One can assume that there is a critical basicity and charge concentration level (OH/Al > 1.3, charge concentration ≤ 0.26 μequiv./mg_{salt}) at which the coagulant is not able to sufficiently destabilize the disperse system in BF-MBR. Apparently, the function of filtration enhancement versus the coagulant basicity has a quadratic polynomial character with the maximum reached at the medium basicity level, which requires further investigations.

Prepolymerized aluminium chloride of medium basicity demonstrated the greatest extent of membrane fouling reduction, which can be explained by its highest bearing charge, and, hence the highest potential to neutralize the oppositely charged foulants. In addition, prepolymerized aluminium chloride of medium basicity alleviated fouling by the increase of foulant relative hydrophobicity, reduction of the concentration of soluble microbial products and the increase of the size of particulate matter. However, we attribute its outstanding efficiency mainly to the dominance of a complex adsorption/charge neutralization mechanism since, in case of non-prepolymerized aluminium or iron (III) sulphate, neither the increase of the particle size nor the combination of the SMPs removal with the increase of floc relative hydrophobicity alone could provide a sufficient level of flux enhancement.

Thus, the conclusions by Ivanovic and Leiknes [22,35], that flux enhancement occurs merely through the increase of the particle size and reduction of the content of submicron particles with practically no role of charge neutralization mechanism cannot be supported without going into the conflict. However, their results might be explained by the applied pH of coagulation, which apparently was unfavourable for coagulation (below the optimum levels). Thus, this entails the incomplete hydrolysis of $Fe(H_2O)_6^{3+}$ and prepolymerized aluminium species (like $Al_{13}O_4(OH)^{7+}$) and, hence, the incomplete destabilization of the disperse system. As shown in the current work, Fe-based coagulants can work at a more acidic pH, than Al-based coagulants and therefore can provide better coagulation and fouling mitigation, which was observed in the mentioned studies [22,35].

Since adsorption/charge neutralization was found to be the principal mechanism during chemical flux enhancement in BF-MBR system, no additional testing is required to evaluate the fouling alleviation propensity of the new inorganic coagulants in this system, which will help to simplify the testing procedure and bring the technology to the next level.

The optimization analysis revealed the significance of MLSS, coagulant dose, temperature and pH in the filtration processes. It is noteworthy that the developed optimization approach can be applied to predict the filtration performance, specifying the factorial levels for a single variable outside the defined factorial settings, since the valid range for coded values is −5–+5. This can be very useful during the operational routine, taking into account the fluctuations in the characteristics of the incoming wastewater. While wastewater temperature is barely controllable in practice and mostly varies with the season (warm/cold) [145] and the intensity/frequency of the storm events [146], its potential impact on the BF-MBR system can be predicted, applying the derived models. The adverse effect of the low temperatures can be minimized by adjusting the levels of the other parameters in the system, according to the presented optimization analysis. As shown in our previous work [42], MLSS can be regulated by adjusting sludge retention time in the decentralized BF-MBR systems. Meanwhile, the coagulant dose and pH of mixed liquor are readily adjustable by changing the settings of the relevant dosing stations.

Different future research directions can be singled out. The developed multivariate chemometric approach can be used for the development of the sensors for fouling monitoring and prediction based on the biomass properties in BF-MBR.

In this work, mixed liquor was considered as substrate and all the mechanisms of fouling mitigation in BF-MBR were studied in relation to the substrate. However, further studies in this area can focus on the composition of the biocoenosis in BF-MBR to develop a targeting chemical influence on its fouling propensity, depending on the content.

The current research was focused on the use of individual inorganic coagulants in the separation chamber of BF-MBR; however, they can be applied in pairs with organic flocculants and the potential of their dosing in MBRR part should be checked.

If the BF-MBR is designed to biologically remove phosphorus and nitrogen in MBBR part, with the use of anaerobic and anoxic stages, it might affect fouling intensity and mitigation in the BF-MBR, which also requires further investigation.

5. Conclusions

The current research conducted the comparative study of prepolymerized and non-prepolymerized inorganic coagulants through the chemometric approach to membrane fouling control and optimization of membrane filtration, resulting in the development of the concept of chemical flux enhancement in the biofilm membrane bioreactor based on the adsorption/charge neutralization mechanism.

Introduction of prepolymerized aluminium chloride of medium and high basicity, as well as aluminium or iron (III) sulphate to the membrane separation stage of the biofilm membrane bioreactor, provides equally high turbidity removal and residual orthophosphate concentration below the allowable limits. Two prepolymerized aluminium coagulants and iron (III) sulphate provided the highest removal of dissolved organic matter. Application of prepolymerized aluminium coagulants in the optimum dosage region resulted in the residual aluminium concentrations below the allowable limits (0–0.03 mgAl/L), which is favourable for the environment.

In contrast to the non-prepolymerized coagulants, prepolymerized aluminium coagulants were much more efficient with respect to flux enhancement. They demonstrated the greatest fouling mitigation extent: 120.0 min of filtration time and the maximum increase of the average normalized permeability by 155.0–198.0%, which corresponds to a tenfold increase in filtration length of the membrane separation cycle and 30.0–56.0% increase in net flux (depending on the operational period) of the BF-MBR pilot system.

The prepolymerized aluminium chloride of medium basicity had the highest bearing positive charge and demonstrated the greatest extent of fouling alleviation, which suggests the significance of the adsorption/charge neutralization mechanism in the flux enhancement in biofilm membrane bioreactor, while in case of non-prepolymerized iron (III) or aluminium sulphate the combination of the dissolve organic matter removal with the increase of floc relative hydrophobicity or the increase in particle size were not enough.

The efficiency of the studied coagulants can be improved by applying optimum pH levels of coagulation: 5.5–6.0 for prepolymerized aluminium chloride coagulants, 4.5 for aluminium sulphate and 3.8–4.1 for iron (III) sulphate.

The developed PLS-regression model demonstrated the significance of the selected mixed liquor parameters and the response functions for estimation and prediction of fouling intensity. The cross-validation of the derived model indicated low uncertainty and negligible bias of the predictions; and hence, high reliability of the model, allowing its further implementation.

The analysis of the two-level factorial design of the experiment provided the models for estimation and prediction of the fouling intensity and the levels of the factors for optimization of membrane filtration using the prepolymerized aluminium chloride with medium basicity. The validation analysis, point prediction and confirmation for the defined factor settings proved the absence of outliers, stability and reliability of the derived optimization models.

The models can be used to adjust operational parameters of the BF-MBR pilot system according to the characteristics of biomass, which will improve filtration efficiency and stability in the system.

The results of this research will simplify the evaluation of the flux enhancers in decentralized BF-MBR systems and can serve as the basis for the automated process control of BF-MBR, which is another step towards the increase of filtration efficiency, operation improvement and the reduction of maintenance costs.

Supplementary Materials: The following are available online at http://www.mdpi.com/2073-4441/11/3/446/s1, Figure S1: Preliminary examination of the influence of: (**a**) coagulant dose; (**b**) pH; (**c**) temperature on the average permeability, coloured by MLSS, Figure S2: A negative correlation between capillary suction time (CST)

and relative hydrophobicity (RH) earlier obtained for BF-MBR mixed liquor by Kulesha et al. [42], Table S1: Characterization of particle properties by particle size distribution [48–52], Table S2: Optimum pH ranges and the corresponding parameters of the system, Table S3: Optimum dosages at the corrected pH values applying tested coagulants, Table S4: Optimum dosages and the corresponding levels of the monitored parameters during TRT with pH adjustment, Table S5: The obtained optimum concentration ranges of the added coagulants with and without the pH correction, Table S6: Point prediction and confirmation for the tested factor settings.

Author Contributions: O.K. and Z.M. conceived and designed the experiments; O.K. performed the experiments under the supervision of Z.M. and analysed the data; O.K. performed statistical and image analysis under the supervision of K.K; K.K. contributed to the discussion of the article; H.R. contributed reagents, materials and analysis tools and contributed to the discussion of the article; O.K. wrote the paper with advice from Z.M, K.K. and H.R.

Funding: This research was co-funded by the CE-MBR project (project number: 8650000006MH) and the Erasmus+ Program of the European Union (project number: 561755-EPP-1-2015-1-NOEPPKA2-CBHE-JP).

Acknowledgments: Authors express their gratitude to Stella Saliu for her input as Erasmus+ exchange student and Sven Andreas Högfeldt for his guidance on size exclusion chromatography.

Conflicts of Interest: The authors declare no conflict of interest. The founding sponsors had no role in the design of the study; in the collection, analyses or interpretation of data; in the writing of the manuscript and in the decision to publish the results.

References

1. European Commission. *Regulation of the European Parliament and the Council on Minimum Requirements for Water Reuse*; European Commission: Brussels, Belgium, 2018; Volume 169, p. 28.
2. European Commission. *Report on the Review of the European Water Scarcity and Droughts Policy*; European Commission: Brussels, Belgium, 2012.
3. Hankins, N.P.; Singh, R. *Emerging Membrane Technology for Sustainable Water Treatment*; Marinakis, K., Ed.; Elsevier: Amsterdam, The Netherlands; Oxford, UK; Cambridge, MA, USA, 2016; ISBN 978-0-444-63312-5.
4. Maletskyi, Z.; Kulesha, O.; Ratnaweera, H.C. Comparison of Al- and Fe-based Membrane Fouling Reducers for BioFilm Membrane BioReactor. In Proceedings of the Euromembrane 2018, Valencia, Spain, 9–13 July 2018.
5. United States Environmental Protection Agency Water Reuse and Recycling: Community and Environmental Benefits. Available online: https://www3.epa.gov/region9/water/recycling/ (accessed on 22 January 2019).
6. Bernal, D.P.; Restrepo, I. Key issues for decentralization in municipal wastewater treatment. In *12th Edition of the World Wide Workshop for Young Environmental Scientists (WWW-YES-2012)—Urban Waters: Resource or Risks?* HAL-ENPC: Arcueil, France, 2012.
7. Kulesha, O.; Maletskyi, Z.; Ratnaweera, H. State-of-the-art of membrane flux enhancement in membrane bioreactor. *Cogent Eng.* **2018**, *5*, 1–30. [CrossRef]
8. Meng, F.; Zhang, S.; Oh, Y.; Zhou, Z.; Shin, H.-S.; Chae, S.-R. Fouling in membrane bioreactors: An updated review. *Water Res.* **2017**, *114*, 151–180. [CrossRef] [PubMed]
9. Jørgensen, M.K.; Nierychlo, M.; Nielsen, A.H.; Larsen, P.; Christensen, M.L.; Nielsen, P.H. Unified understanding of physico-chemical properties of activated sludge and fouling propensity. *Water Res.* **2017**, *120*, 117–132. [CrossRef] [PubMed]
10. Zhu, J.; Hou, J.; Zhang, Y.; Tian, M.; He, T.; Liu, J.; Chen, V. Polymeric antimicrobial membranes enabled by nanomaterials for water treatment. *J. Membr. Sci.* **2018**, *550*, 173–197. [CrossRef]
11. Zheng, Y.; Zhang, W.; Tang, B.; Ding, J.; Zheng, Y.; Zhang, Z. Membrane fouling mechanism of biofilm-membrane bioreactor (BF-MBR): Pore blocking model and membrane cleaning. *Bioresour. Technol.* **2018**, *250*, 398–405. [CrossRef] [PubMed]
12. Ivanovic, I.; Leiknes, T.O. The biofilm membrane bioreactor (BF-MBR)—A review. *Desalin. Water Treat.* **2012**, *37*, 288–295. [CrossRef]
13. Ødegaard, H. Innovations in wastewater treatment: The moving bed biofilm process. *Water Sci. Technol.* **2006**, *53*, 17–33. [CrossRef] [PubMed]
14. Phattaranawik, J.; Leiknes, T. Study of Hybrid Vertical Anaerobic Sludge-Aerobic Biofilm Membrane Bioreactor for Wastewater Treatment. *Water Environ. Res.* **2010**, *82*, 273–280. [CrossRef] [PubMed]
15. Sun, C.; Leiknes, T.; Fredriksen, R.H.; Riviere, E. Comparison of membrane filtration performance between biofilm-MBR and activated sludge-MBR. *Desalin. Water Treat.* **2012**, *48*, 285–293. [CrossRef]

16. Leiknes, T.; Ødegaard, H. The development of a biofilm membrane bioreactor. *Desalination* **2007**, *202*, 135–143. [CrossRef]
17. Dalmau, M.; Atanasova, N.; Gabarrón, S.; Rodriguez-Roda, I.; Comas, J. Comparison of a deterministic and a data driven model to describe MBR fouling. *Chem. Eng. J.* **2015**, *260*, 300–308. [CrossRef]
18. Deng, L.; Guo, W.; Ngo, H.H.; Zhang, H.; Wang, J.; Li, J.; Xia, S.; Wu, Y. Biofouling and control approaches in membrane bioreactors. *Bioresour. Technol.* **2016**, *221*, 656–665. [CrossRef] [PubMed]
19. Germain, E.; Stephenson, T. Biomass characteristics, aeration and oxygen transfer in membrane bioreactors: Their interrelations explained by a review of aerobic biological processes. *Rev. Environ. Sci. Biotechnol.* **2005**, *4*, 223–233. [CrossRef]
20. Sun, F.Y.; Li, P.; Li, J.; Li, H.J.; Ou, Q.M.; Sun, T.T.; Dong, Z.J. Hybrid biofilm-membrane bioreactor (Bf-MBR) for minimization of bulk liquid-phase organic substances and its positive effect on membrane permeability. *Bioresour. Technol.* **2015**, *198*, 772–780. [CrossRef] [PubMed]
21. Nouri, N.; Mehrnia, M.R.; Sarrafzadeh, M.H.; Nabizadeh, R. Performance of membrane bioreactor in presence of flocculants. *Desalin. Water Treat.* **2013**, *52*, 2933–2938. [CrossRef]
22. Ivanovic, I.; Leiknes, T.O. Improved Performance through Particle Surface Modifications by Coagulation with Inorganic Coagulants in a Biofilm Membrane Bioreactor (BF-MBR). *Sep. Sci. Technol.* **2012**, *48*, 288–294. [CrossRef]
23. Deng, L.; Guo, W.; Hao, H.; Farzana, M.; Zuthi, R.; Zhang, J.; Liang, S.; Li, J.; Wang, J.; Zhang, X. Membrane fouling reduction and improvement of sludge characteristics by bioflocculant addition in submerged membrane bioreactor. *Sep. Purif. Technol.* **2015**, *156*, 450–458. [CrossRef]
24. Iversen, V.; Mehrez, R.; Horng, R.Y.; Chen, C.H.; Meng, F.; Drews, A.; Lesjean, B.; Ernst, M.; Jekel, M.; Kraume, M. Fouling mitigation through flocculants and adsorbents addition in membrane bioreactors: Comparing lab and pilot studies. *J. Membr. Sci.* **2009**. [CrossRef]
25. Wu, J.; Huang, X. Effect of dosing polymeric ferric sulfate on fouling characteristics, mixed liquor properties and performance in a long-term running membrane bioreactor. *Sep. Purif. Technol.* **2008**, *63*, 45–52. [CrossRef]
26. Wang, Z.; Wu, Z.; Mai, S.; Yang, C.; Wang, X.; An, Y.; Zhou, Z. Research and applications of membrane bioreactors in China: Progress and prospect. *Sep. Purif. Technol.* **2008**, *62*, 249–263. [CrossRef]
27. Ji, J.; Li, J.; Qiu, J.; Li, X. Polyacrylamide-starch composite flocculant as a membrane fouling reducer: Key factors of fouling reduction. *Sep. Purif. Technol.* **2014**, *131*, 1–7. [CrossRef]
28. Xiao, Y.; Waheed, H.; Xiao, K.; Hashmi, I.; Zhou, Y. In tandem effects of activated carbon and quorum quenching on fouling control and simultaneous removal of pharmaceutical compounds in membrane bioreactors. *Chem. Eng. J.* **2018**, *341*, 610–617. [CrossRef]
29. Zhang, H.; Sun, B.; Zhao, X.; Gao, Z. Effect of ferric chloride on fouling in membrane bioreactor. *Sep. Purif. Technol.* **2008**, *63*, 341–347. [CrossRef]
30. Guo, W.; Ngo, H.H.; Vigneswaran, S.; Dharmawan, F.; Nguyen, T.T.; Aryal, R. Effect of different flocculants on short-term performance of submerged membrane bioreactor. *Sep. Purif. Technol.* **2010**, *70*, 274–279. [CrossRef]
31. Liu, Y.Y.; Zhang, W.J.; Yang, X.Y.; Xiao, P.; Wang, D.S.; Song, Y. Advanced treatment of effluent from municipal WWTP with different metal salt coagulants: Contaminants treatability and floc properties. *Sep. Purif. Technol.* **2013**, *120*, 123–128. [CrossRef]
32. Holbrook, R.D.; Higgins, M.J.; Murthy, S.N.; Fonseca, A.D.; Fleischer, E.J.; Daigger, G.T.; Grizzard, T.J.; Love, N.G.; Novak, J.T. Effect of alum addition on the performance of submerged membranes for wastewater treatment. *Water Environ. Res.* **2003**, *76*, 2699–2702. [CrossRef]
33. Lee, J.C.; Kim, J.S.; Kang, I.J.; Cho, M.H.; Park, P.K.; Lee, C.H. Potential and limitations of alum or zeolite addition to improve the performance of a submerged membrane bioreactor. *Water Sci. Technol.* **2001**, *43*, 59–66. [CrossRef] [PubMed]
34. Song, K.G.; Kim, Y.; Ahn, K.H. Effect of coagulant addition on membrane fouling and nutrient removal in a submerged membrane bioreactor. *Desalination* **2008**, *221*, 467–474. [CrossRef]
35. Ivanovic, I.; Leiknes, T. Effect of addition of different additives on overall performance of biofilm-MBR (BF-MBR). *Desalin. Water Treat.* **2011**, *34*, 129–135. [CrossRef]
36. Ødegaard, H.; Fettig, J.; Ratnaweera, H.C. *Coagulation with Prepolymerized Metal Salts*; Hahn, H.H., Klute, R., Eds.; Chemical Water and Wastewater Treatment; Springer: Berlin/Heidelberg, Germany, 1990; ISBN 978-3-642-76093-8.

37. Gregory, J.; Duan, J. Hydrolyzing metal salts as coagulants. *Pure Appl. Chem.* **2001**, *73*, 2017–2026. [CrossRef]
38. Wu, J.; Chen, F.; Huang, X.; Geng, W.; Wen, X. Using inorganic coagulants to control membrane fouling in a submerged membrane bioreactor. *Desalination* **2006**, *197*, 124–136. [CrossRef]
39. Chen, W.; Liu, J. The possibility and applicability of coagulation-MBR hybrid system in reclamation of dairy wastewater. *Desalination* **2012**, *285*, 226–231. [CrossRef]
40. Gkotsis, P.K.; Batsari, E.L.; Peleka, E.N.; Tolkou, A.K.; Zouboulis, A.I. Fouling control in a lab-scale MBR system: Comparison of several commercially applied coagulants. *J. Environ. Manag.* **2017**, *203*, 838–846. [CrossRef] [PubMed]
41. Bratby, J. *Coagulation and Flocculation in Water and Wastewater Treatment*, 2nd ed.; IWA Publishing: London, UK; Seattle, WA, USA, 2006; ISBN 9781843391067.
42. Kulesha, O.; Maletskyi, Z.; Ratnaweera, H. Multivariate Chemometric Analysis of Membrane Fouling Patterns in Biofilm Ceramic Membrane Bioreactor. *Water* **2018**, *10*, 982. [CrossRef]
43. Lee, W.-N.; Chang, I.-S.; Hwang, B.-K.; Park, P.-K.; Lee, C.-H.; Huang, X. Changes in biofilm architecture with addition of membrane fouling reducer in a membrane bioreactor. *Process Biochem.* **2007**, *42*, 655–661. [CrossRef]
44. Yeon, K.-M.; Cheong, W.-S.; Oh, H.-S.; Lee, W.-N.; Hwang, B.-K.; Lee, C.-H.; Beyenal, H.; Lewandowski, Z. Quorum Sensing: A New Biofouling Control Paradigm in a Membrane Bioreactor for Advanced Wastewater Treatment. *Environ. Sci. Technol.* **2009**, *43*, 380–385. [CrossRef] [PubMed]
45. Oh, H.-S.; Yeon, K.-M.; Yang, C.-S.; Kim, S.-R.; Lee, C.-H.; Park, S.Y.; Han, J.Y.; Lee, J.-K. Control of membrane biofouling in MBR for wastewater treatment by quorum quenching bacteria encapsulated in microporous membrane. *Environ. Sci. Technol.* **2012**, *46*, 4877–4884. [CrossRef] [PubMed]
46. International Organization for Standardization. *International Standard: ISO 15705:2002. Water Quality—Determination of the Chemical Oxygen Demand Index (ST-COD)—Small-Scale Sealed-Tube Method*; International Organization for Standardization: Geneva, Switzerland, 2002; p. 18.
47. ImageJ: Image Processing and Analysis in Java. Available online: https://imagej.nih.gov/ij/ (accessed on 1 February 2019).
48. Rawle, A. Basic Principles of Particle Size Analysis. Available online: http://cat.inist.fr/?aModele=afficheN&cpsidt=14620810 (accessed on 20 November 2018).
49. Innopharma Technology. A Guide to D-Values in Pharmaceutical Particle Characterisation. Available online: http://www.innopharmalabs.com/tech/applications-and-processes/particle-size-distribution (accessed on 20 November 2018).
50. Horiba Ltd. A Guidebook to Particle Size Analysis. Available online: https://www.horiba.com/fileadmin/uploads/Scientific/Documents/PSA/PSA_Guidebook.pdf (accessed on 20 November 2018).
51. Malvern Instruments Limited. A Basic Guide to Particle Characterization. Available online: https://www.cif.iastate.edu/sites/default/files/uploads/Other_Inst/ParticleSize/ParticleCharacterizationGuide.pdf (accessed on 20 November 2018).
52. Malvern Instruments Ltd. Manual 0101. Available online: Pmbrc.org/index.php/download_file/view/190/ (accessed on 20 November 2018).
53. Micrometrix Corporation. *Particle Charge Analyser. Operating Manual*; Micrometrix Corporation: Suwanee, GA, USA, 2012; p. 19.
54. American Public Health Association; Water Environment Federation; American Water Works Association. *Standard Methods for the Examination of Water and Wastewater*, 22nd ed. Rice, E.W., Baird, R.B., Eaton, A.D., Clesceri, L.S., Eds.; American Public Health Association: Washington, DC, USA, 2012; ISBN 9780875530130.
55. CAMO. *The Unscrambler Tutorials. CAMO Process AS 2006*; CAMO Software AS: Oslo, Norway, 2006; p. 179.
56. Olivieri, A.C. *Introduction to Multivariate Calibration: A Practical Approach*; Springer: Cham, Switzerland, 2018; ISBN 9783319970974.
57. Van den Broeck, R.; Krzeminski, P.; Van Dierdonck, J.; Gins, G.; Lousada-Ferreira, M.; Van Impe, J.F.M.; van der Graaf, J.H.J.M.; Smets, I.Y.; van Lier, J.B. Activated sludge characteristics affecting sludge filterability in municipal and industrial MBRs: Unraveling correlations using multi-component regression analysis. *J. Membr. Sci.* **2011**, *378*, 330–338. [CrossRef]

58. Wold, S.; Sjostrom, M.; Eriksson, L. PLS-regression: A basic tool of chemometrics. *Chemom. Intell. Lab. Syst.* **2001**, *58*, 109–130. [CrossRef]
59. Bratby, J. *Coagulation and Flocculation in Water and Wastewater Treatment*, 3rd ed.; IWA Publishing: London, UK, 2016; ISBN 9781780407500.
60. Ratnaweera, H.C. Influence of the Degree of Coagulant Prepolymerization on Wastewater Coagulation Mechanisms. Ph.D. Thesis, The University of Trondheim. The Norwegian Institute of Technology, Trondheim, Norway, 1991.
61. Stumm, W.; Morgan, J.J. Chemical Aspects of Coagulation. *J. Am. Water Works Assoc.* **1962**, *54*, 971–991. [CrossRef]
62. Stumm, W.; O'Melia, C. Stoichiometry of coagulation. *Am. Water Work. Assoc.* **1968**, *60*, 514–539. [CrossRef]
63. Meyn, T.; Leiknes, T.; Ødegaard, H. Coagulation/flocculation—Ceramic membrane filtration for removal of natural organic matter (NOM) under Norwegian conditions. In Proceedings of the IWA Conference on Membranes for Water and Wastewater Treatment, Harrogate, UK, 15–17 May 2007.
64. Liang, Z.; Wang, Y.; Zhou, Y.; Liu, H.; Wu, Z. Polishing treatment of molasses wastewater with iron salts: The role of counter-ions. *Water Environ. Res.* **2009**, *81*, 2293–2298. [CrossRef] [PubMed]
65. Ng, M.; Liana, A.E.; Liu, S.; Lim, M.; Chow, C.W.K.; Wang, D.; Drikas, M.; Amal, R. Preparation and characterisation of new-polyaluminum chloride-chitosan composite coagulant. *Water Res.* **2012**, *46*, 4614–4620. [CrossRef] [PubMed]
66. American Water College Zeta Potential—Coagulation and Flocculation Lecture. Available online: https://thewaternetwork.com/article-FfV/zeta-potential-coagulation-and-flocculation-lecture-video-gUbFb9OUygf-evijymdc6g (accessed on 29 November 2018).
67. Hall, E.S.; Packham, R.F. Coagulation of Organic Color With Hydrolyzing Coagulants. *J. Am. Water Work. Assoc.* **1965**, *57*, 1149–1166. [CrossRef]
68. Guminska, J.; Klos, M. Effect of Polyaluminium Chlorides Overdosage on Effectiveness of Coagulation and Filtration. *Environ. Prot. Eng.* **2015**, *41*, 5–14. [CrossRef]
69. Bachand, P.A.M.; Bachand, S.M.; Lopus, S.E.; Heyvaert, A.; Werner, I. Treatment with chemical coagulants at different dosing levels changes ecotoxicity of stormwater from the Tahoe basin, California, USA. *J. Environ. Sci. Heal. Part A Toxic/Hazard. Subst. Environ. Eng.* **2010**, *45*, 137–154. [CrossRef] [PubMed]
70. Wang, Z.; Wu, Z.; Tang, S. Impact of temperature seasonal change on sludge characteristics and membrane fouling in a submerged membrane bioreactor. *Sep. Sci. Technol.* **2010**, *45*, 920–927. [CrossRef]
71. Sobeck, D.C.; Higgins, M.J. Examination of three theories for mechanisms of cation-induced bioflocculation. *Water Res.* **2002**, *36*, 527–538. [CrossRef]
72. Klute, R. Destabilization and Aggregation in Turbulent Pipe Flow. *Chem. Water Wastewater Treat.* **1990**, 33–54. [CrossRef]
73. Drews, A. Membrane fouling in membrane bioreactors-Characterisation, contradictions, cause and cures. *J. Membr. Sci.* **2010**, *363*, 1–28. [CrossRef]
74. Miller, D.J.; Kasemset, S.; Paul, D.R.; Freeman, B.D. Comparison of membrane fouling at constant flux and constant transmembrane pressure conditions. *J. Membr. Sci.* **2014**, *454*, 505–515. [CrossRef]
75. Council of the European Communities. *Directive Concerning Urban Waste Water Treatment (91/271/EEC)*; Urban Waste Water Directive: Brussels, Belgium, 1991; pp. 40–52.
76. Ratnaweera, H.; Ødegaard, H.; Fettig, J. Coagulation with prepolymerised aluminium salts and their influence on particle and phosphate removal. *Water Sci. Technol.* **1992**, *6*, 1229–1237. [CrossRef]
77. Zhang, X.; Fan, L.; Roddick, F.A. Feedwater coagulation to mitigate the fouling of a ceramic MF membrane caused by soluble algal organic matter. *Sep. Purif. Technol.* **2014**, *133*, 221–226. [CrossRef]
78. United States Environmental Protection Agency. *EPA Ambient Water Quality Criteria for Aluminium*; Office of Water Regulations and Standards Criteria and Standards Division: Washington, DC, USA, 1988.
79. European Commission. *EU-Level Instruments on Water Reuse: Final Report to Support the Commission's Impact Assessment*; European Commission: Brussels, Belgium, 2016.
80. Eignor, D. Draft National 304(a) Aluminum Aquatic Life Criteria. Available online: https://www.epa.gov/sites/production/files/2017-09/documents/aluminum-webinar-9192017.pdf (accessed on 1 December 2018).

81. Zhang, Z.; Wang, Y.; Leslie, G.L.; Waite, T.D. Effect of ferric and ferrous iron addition on phosphorus removal and fouling in submerged membrane bioreactors. *Water Res.* **2015**, *69*, 210–222. [CrossRef] [PubMed]
82. Wang, X.-M.; Waite, T.D. Role of gelling soluble and colloidal microbial products in membrane fouling. *Environ. Sci. Technol.* **2009**, *43*, 9341–9347. [CrossRef] [PubMed]
83. Dulko, J.M. Stable Concentrated Polyaluminium Chlorosilicate Solutions. US 2016/0244345 A1, issued 2016. US 2016/0244345 A1, 2016. [CrossRef]
84. Dulko, J.M. Stable Concentrated Polyaluminum Chlorosilicate Solutions. WO 2016/134277 Al, 2016. Available online: https://patents.google.com/patent/WO2016134277A1 (accessed on 28 February 2018).
85. Zouboulis, A.I.; Tzoupanos, N.D. Polyaluminium silicate chloride-A systematic study for the preparation and application of an efficient coagulant for water or wastewater treatment. *J. Hazard. Mater.* **2009**, *162*, 1379–1389. [CrossRef] [PubMed]
86. Gao, B.Y.; Yue, Q.Y.; Wang, B.J.; Chu, Y.B. Poly-aluminum-silicate-chloride (PASiC)—A new type of composite inorganic polymer coagulant. *Colloids Surfaces A Physicochem. Eng. Asp.* **2003**, *229*, 121–127. [CrossRef]
87. Zhang, P.; Hahn, H.H.; Hoffmann, E.; Zeng, G. Influence of some additives to aluminium species distribution in aluminium coagulants. *Chemosphere* **2004**, *57*, 1489–1494. [CrossRef] [PubMed]
88. Tzoupanos, N.D.; Zouboulis, A.I.; Tsoleridis, C.A. A systematic study for the characterization of a novel coagulant (polyaluminium silicate chloride). *Colloids Surf. A Physicochem. Eng. Asp.* **2009**, *342*, 30–39. [CrossRef]
89. Ratnaweera, H.; Fettig, J. State of the art of online monitoring and control of the coagulation process. *Water (Switzerland)* **2015**, *7*, 6574–6597. [CrossRef]
90. Adgar, A.; Cox, C.S.; Jones, C.A. Enhancement of coagulation control using the streaming current detector. *Bioprocess Biosyst. Eng.* **2005**, 349–357. [CrossRef] [PubMed]
91. Brookes, A.; Judd, S.; Reid, E.; Germain, E.; Smith, S.; Alvarez-Vazquez, H.; Le-Clech, P.; Stephenson, T.; Turra, E.; Jefferson, B. Biomass characterisation in membrane bioreactors. In Proceedings of the International Membrane Science and Technology Conference (IMSTEC), Sydney, Australia, 10–14 November 2003.
92. Striegel, A.M. Size-exclusion chromatography. In *Liquid Chromatography: Fundamentals and Instrumentation: Second Edition*; Elsevier: Gaithersburg, MD, USA, 2017; pp. 193–224. ISBN 9780128053935.
93. Montgomery, D.C. Design and Analysis of Experiments, 15th ed.John Wiley & Sons, Inc.: Scottsdale, AZ, USA, 1997.
94. Stat-Ease Inc. Design-Expert 11.1.0. Documentation. Tutorials. Available online: https://www.statease.com/docs/v11/index.html (accessed on 31 October 2018).
95. Ogee, A.; Ellis, M.; Stone, B.K.; Scibilia, B.; Pammer, C.; Steele, C. MiniTab 18: What Are T Values and P Values in Statistics? Available online: https://blog.minitab.com/blog/statistics-and-quality-data-analysis/what-are-t-values-and-p-values-in-statistics (accessed on 12 January 2019).
96. Mendenhall, W.; Sincich, T. *A Second Course in Statistics. Regression Analysis*, 7th ed.; Lynch, D., Ed.; Pearson Education, Inc.: Boston, MA, USA, 2012; ISBN 0-321-69169-5.
97. Winter, B. The F Distribution and the Basic Principle behind ANOVAs. Available online: http://www.bodowinter.com/tutorial/bw_anova_general.pdf (accessed on 1 November 2018).
98. The Bayes Information Criterion (BIC). Available online: http://www-math.mit.edu/~{}rmd/650/bic.pdf (accessed on 1 November 2018).
99. Merisaari, H.; Jambor, I.; Jødal, L.; Oikonen, V. Akaike Information Criterium (AIC) in Model Selection. Available online: http://www.turkupetcentre.net/petanalysis/model_aic.html (accessed on 1 November 2018).
100. Montgomery, D.C. *Design and Analysis of Experiments*, 8th ed.; Ratts, L., Melhorn, A., Eds.; John Wiley & Sons, Inc.: Hoboken, NJ, USA, 2013; ISBN 9781118146927.
101. Hair, J.F.; Black, W.C.; Babin, B.J.; Anderson, R.E. *Multivariate Data Analysis. Pearson New International Edition*, 7th ed.; Pearson Education Limited: Harlow, UK, 2014; ISBN 9781292021904.
102. Azami, H.; Sarrafzadeh, M.H.; Mehrnia, M.R. Influence of sludge rheological properties on the membrane fouling in submerged membrane bioreactor. *Desalin. Water Treat.* **2011**, *34*, 117–122. [CrossRef]
103. Meng, F.; Shi, B.; Yang, F.; Zhang, H. Effect of hydraulic retention time on membrane fouling and biomass characteristics in submerged membrane bioreactors. *Bioprocess Biosyst. Eng.* **2007**, *30*, 359–367. [CrossRef] [PubMed]

104. Chang, I.S.; Kim, S.N. Wastewater treatment using membrane filtration—Effect of biosolids concentration on cake resistance. *Process Biochem.* **2005**, *40*, 1307–1314. [CrossRef]
105. Le-Clech, P.; Chen, V.; Fane, T.A.G. Fouling in membrane bioreactors used in wastewater treatment. *J. Membr. Sci.* **2006**, *284*, 17–53. [CrossRef]
106. Ji, L.; Zhou, J. Influence of aeration on microbial polymers and membrane fouling in submerged membrane bioreactors. *J. Membr. Sci.* **2006**, *276*, 168–177. [CrossRef]
107. Hernandez Rojas, M.E.; Van Kaam, R.; Schetrite, S.; Albasi, C. Role and variations of supernatant compounds in submerged membrane bioreactor fouling. *Desalination* **2005**, *179*, 95–107. [CrossRef]
108. Xie, W.M.; Ni, B.J.; Sheng, G.P.; Seviour, T.; Yu, H.Q. Quantification and kinetic characterization of soluble microbial products from municipal wastewater treatment plants. *Water Res.* **2016**, *88*, 703–710. [CrossRef] [PubMed]
109. Tu, X.; Zhang, S.; Xu, L.; Zhang, M.; Zhu, J. Performance and fouling characteristics in a membrane sequence batch reactor (MSBR) system coupled with aerobic granular sludge. *Desalination* **2010**, *261*, 191–196. [CrossRef]
110. Deng, L.; Guo, W.; Ngo, H.H.; Zhang, J.; Liang, S.; Xia, S.; Zhang, Z.; Li, J. A comparison study on membrane fouling in a sponge-submerged membrane bioreactor and a conventional membrane bioreactor. *Bioresour. Technol.* **2014**, *165*, 69–74. [CrossRef] [PubMed]
111. Zhang, H.; Yu, H.; Zhang, L.; Song, L. Bioresource Technology Stratification structure of polysaccharides and proteins in activated sludge with different aeration in membrane bioreactor. *Bioresour. Technol.* **2015**, *192*, 361–366. [CrossRef] [PubMed]
112. Johir, M.A.H.; Vigneswaran, S.; Sathasivan, A.; Kandasamy, J.; Chang, C.Y. Effect of organic loading rate on organic matter and foulant characteristics in membrane bio-reactor. *Bioresour. Technol.* **2012**, *113*, 154–160. [CrossRef] [PubMed]
113. Qin, L.; Zhang, G.; Meng, Q.; Zhang, H.; Xu, L.; Lv, B. Enhanced submerged membrane bioreactor combined with biosurfactant rhamnolipids: Performance for frying oil degradation and membrane fouling reduction. *Bioresour. Technol.* **2012**, *126*, 314–320. [CrossRef] [PubMed]
114. Shen, Y.; Zhao, W.; Xiao, K.; Huang, X. A systematic insight into fouling propensity of soluble microbial products in membrane bioreactors based on hydrophobic interaction and size exclusion. *J. Membr. Sci.* **2010**, *346*, 187–193. [CrossRef]
115. Pramanik, B.K.; Roddick, F.A.; Fan, L. Impact of biological activated carbon pre-treatment on the hydrophilic fraction of effluent organic matter for mitigating fouling in microfiltration. *Environ. Technol.* **2018**, *39*, 2243–2250. [CrossRef] [PubMed]
116. Mu, S.; Wang, S.; Liang, S.; Xiao, K.; Fan, H.; Han, B.; Liu, C.; Wang, X.; Huang, X. Effect of the relative degree of foulant "hydrophobicity" on membrane fouling. *J. Membr. Sci.* **2019**, *570–571*, 1–8. [CrossRef]
117. Ivanovic, I.; Leiknes, T.O.; Ødegaard, H. Fouling control by reduction of submicron particles in a BF-MBR with an integrated flocculation zone in the membrane reactor. *Sep. Sci. Technol.* **2008**, *43*, 1871–1883. [CrossRef]
118. Tian, Y.; Chen, L.; Zhang, S.; Cao, C.; Zhang, S. Correlating membrane fouling with sludge characteristics in membrane bioreactors: An especial interest in EPS and sludge morphology analysis. *Bioresour. Technol.* **2011**, *102*, 8820–8827. [CrossRef] [PubMed]
119. Tarnacki, K.; Lyko, S.; Wintgens, T.; Melin, T.; Natau, F. Impact of extra-cellular polymeric substances on the filterability of activated sludge in membrane bioreactors for landfill leachate treatment. *Desalination* **2005**, *179*, 181–190. [CrossRef]
120. Rosenberger, S.; Evenblij, H.; Te Poele, S.; Wintgens, T.; Laabs, C. The importance of liquid phase analyses to understand fouling in membrane assisted activated sludge processes—Six case studies of different European research groups. *J. Membr. Sci.* **2005**, *263*, 113–126. [CrossRef]
121. Wu, Z.; Wang, Z.; Zhou, Z.; Yu, G.; Gu, G. Sludge rheological and physiological characteristics in a pilot-scale submerged membrane bioreactor. *Desalination* **2007**, *212*, 152–164. [CrossRef]
122. Pan, J.R.; Su, Y.C.; Huang, C.; Lee, H.C. Effect of sludge characteristics on membrane fouling in membrane bioreactors. *J. Membr. Sci.* **2010**, *349*, 287–294. [CrossRef]
123. Jin, B.; Wilén, B.M.; Lant, P. Impacts of morphological, physical and chemical properties of sludge flocs on dewaterability of activated sludge. *Chem. Eng. J.* **2004**, *98*, 115–126. [CrossRef]

124. Niwa, R.; Yin, T.; Oo, M.H.; Noguchi, H.; Watanabe, T.; Razali, L.Y.; Png, H.Y.; Lay, W.C.L.; Ong, K.A.; Alom, M. Performance of a Full-Scale Ceramic MBR System to Treat Domestic Sewage. *Water Pract. Technol.* **2018**, *13*, 589–593. [CrossRef]
125. Gkotsis, P.K.; Mitrakas, M.M.; Tolkou, A.K.; Zouboulis, A.I. Batch and continuous dosing of conventional and composite coagulation agents for fouling control in a pilot-scale MBR. *Chem. Eng. J.* **2016**, *311*, 255–264. [CrossRef]
126. Fan, F.; Zhou, H.; Husain, H. Identification of wastewater sludge characteristics to predict critical flux for membrane bioreactor processes. *Water Res.* **2006**, *40*, 205–212. [CrossRef] [PubMed]
127. Stumm, W.; Morgan, J.J. *Aquatic Chemistry: Chemical Equilibria and Rates in Natural Waters*, 3rd ed.; Schnoor, J.J., Zehnder, A., Eds.; John Wiley & Soms, Inc.: New York, NY, USA, 1996.
128. Moran, A.P.; Holst, O.; Brennan, P.J.; von Itzstein, M. (Eds.) *Microbial Glycobiology: Structures, Relevance and Applications*; Elsevier Inc.: London, UK; Burlington: San Diego, CA, USA, 2009; ISBN 978-0-12-374546-0.
129. Chen, J.; Lin, H.; Shen, L.; He, Y.; Zhang, M.; Liao, B.Q. Realization of quantifying interfacial interactions between a randomly rough membrane surface and a foulant particle. *Bioresour. Technol.* **2017**, *226*, 220–228. [CrossRef] [PubMed]
130. Zhang, M.; Zhou, X.; Shen, L.; Cai, X.; Wang, F.; Chen, J.; Lin, H.; Li, R.; Wu, X.; Liao, B.Q. Quantitative evaluation of the interfacial interactions between a randomly rough sludge floc and membrane surface in a membrane bioreactor based on fractal geometry. *Bioresour. Technol.* **2017**, *234*, 198–207. [CrossRef] [PubMed]
131. Meng, F.; Zhang, H.; Yang, F.; Zhang, S.; Li, Y.; Zhang, X. Identification of activated sludge properties affecting membrane fouling in submerged membrane bioreactors. *Sep. Purif. Technol.* **2006**, *51*, 95–103. [CrossRef]
132. Ji, J.; Qiu, J.; Wai, N.; Wong, F.S.; Li, Y. Influence of organic and inorganic flocculants on physical-chemical properties of biomass and membrane-fouling rate. *Water Res.* **2010**, *44*, 1627–1635. [CrossRef] [PubMed]
133. Qin, L.; Fan, Z.; Xu, L.; Zhang, G.; Wang, G.; Wu, D.; Long, X.; Meng, Q. A submerged membrane bioreactor with pendulum type oscillation (PTO) for oily wastewater treatment: Membrane permeability and fouling control. *Bioresour. Technol.* **2015**, *183*, 33–41. [CrossRef] [PubMed]
134. Jang, N.; Ren, X.; Choi, K.; Kim, I.S. Comparison of membrane biofouling in nitrification and denitrification for the membrane bioreactor (MBR). *Water Sci. Technol.* **2006**, *53*, 43–49. [CrossRef] [PubMed]
135. Jin, L.; Ong, S.L.; Ng, H.Y. Fouling control mechanism by suspended biofilm carriers addition in submerged ceramic membrane bioreactors. *J. Membr. Sci.* **2013**, *427*, 250–258. [CrossRef]
136. Lykkegaard, M.; Niessen, W.; Bøie, N.; Hove, S.; Koustrup, M.; Halkjær, P. Sludge fractionation as a method to study and predict fouling in MBR systems. *Sep. Purif. Technol.* **2018**, *194*, 329–337. [CrossRef]
137. Remy, M.; Potier, V.; Temmink, H.; Rulkens, W. Why low powdered activated carbon addition reduces membrane fouling in MBRs. *Water Res.* **2010**, *44*, 861–867. [CrossRef] [PubMed]
138. Philippe, N.; Racault, Y.; Stricker, A.E.; Sp, M.; Vanrolleghem, P.A. Modelling the long-term evolution of permeability in a full-scale MBR: Statistical approaches. *Desalination* **2013**, *325*, 7–15. [CrossRef]
139. Naessens, W.; Maere, T.; De Temmerman, L.; Nopens, I. Principal component analysis for monitoring membrane bioreactors: Trend detection, outlier detection and optimization. In Proceedings of the 2013 International Workshop—Membrane Bioreactor for Wastewater Reuse: Fundamental, Design and Operation, Tunis, Tunisia, 12–14 November 2013; pp. 2–5.
140. Kaneko, H.; Funatsu, K. Visualization of Models Predicting Transmembrane Pressure Jump for Membrane Bioreactor. *Ind. Eng. Chem. Res.* **2012**, *51*, 9679–9686. [CrossRef]
141. Choi, B.G.; Cho, J.; Song, K.G.; Maeng, S.K. Correlation between effluent organic matter characteristics and membrane fouling in a membrane bioreactor using advanced organic matter characterization tools. *Desalination* **2013**, *309*, 74–83. [CrossRef]
142. Jacquin, C.; Gambier, N.; Lesage, G.; Heran, M. New insight into fate and fouling behavior of bulk Dissolved Organic Matter (DOM) in a full-scale membrane bioreactor for domestic wastewater treatment. *J. Water Process Eng.* **2018**, *22*, 94–102. [CrossRef]
143. Geladi, P.; Kowalski, B.R. Partial least-squares regression: A tutorial. *Anal. Chim. Acta* **1986**, *185*, 1–17. [CrossRef]
144. Sivchenko, N. Image Analysis in Coagulation Process Control. Ph.D. Thesis, Norwegian University of Life Sciences (NMBU), Ås, Norway, 2017.

145. Wang, X.; Kvaal, K.; Ratnaweera, H. Characterization of influent wastewater with periodic variation and snow melting effect in cold climate area. *Comput. Chem. Eng.* **2017**, *106*, 202–211. [CrossRef]
146. Liltved, H.; Ratnaweera, H.; Plo, B.G. Climate change impacts on activated sludge wastewater treatment: A case study from Norway. *Water Sci. Technol. WST* **2009**, *60*, 533–541. [CrossRef]